EXPERIMENTAL AND COMPUTATIONAL INVESTIGATION OF ZINC OXIDE BASED SURFACE ACOUSTIC WAVE DEVICES

A THESIS

SUBMITTED TO THE DEPARTMENT OF MATERIAL SCIENCE AND NANOTECHNOLOGY

AND THE GRADUATE SCHOOL OF ENGINEERING AND SCIENCE OF BILKENT UNIVERSITY

IN PARTIAL FULFILLMENT OF THE REQUIREMENTS FOR THE DEGREE OF

MASTER OF SCIENCE

By

Elif Özgöztaşı

September, 2014

I certify that I have read this thesis and that in my opinion it is fully adequate, in scope and in quality, as a thesis for the degree of Master of Science.

Assist. Prof. Dr. Ali Kemal Okyay(Advisor)

I certify that I have read this thesis and that in my opinion it is fully adequate, in scope and in quality, as a thesis for the degree of Master of Science.

Assoc. Prof. Dr. Ceyhun Bulutay

I certify that I have read this thesis and that in my opinion it is fully adequate, in scope and in quality, as a thesis for the degree of Master of Science.

Assist. Prof. Dr. Necmi Bıyıklı

Approved for the Graduate School of Engineering and Science:

Prof. Dr. Levent Onural
Director of the Graduate School

ABSTRACT

EXPERIMENTAL AND COMPUTATIONAL INVESTIGATION OF ZINC OXIDE BASED SURFACE ACOUSTIC WAVE DEVICES

Elif Özgöztaşı
M.S. in Material Science and Nanotechnology
Supervisor: Assist. Prof. Dr. Ali Kemal Okyay
September, 2014

Piezoelectric materials are used in different types of transducers such as microphones, accelerometers, speakers, hydrophones, pressure sensors etc. Compared to traditional bulk piezoelectric crystals, thin film piezoelectric materials are promising to realize integrated devices with CMOS technology. Among thin film materials, zinc oxide (ZnO) is attractive due to the giant piezoelectric effect when doped with vanadium.

In this study, we investigate the deposition of thin film ZnO and V-doped ZnO films. Materials characterization of ZnO thin films is performed. We also investigate surface acoustic wave (SAW) devices based on ZnO thin films. SAW devices are formed by a pair of interdigitated transducers (IDTs), input and output IDTs. IDTs are fabricated onto the piezoelectric thin film. Applied oscillating electric field from input IDT creates surface acoustic waves in the piezoelectric thin film and these acoustic waves are converted back into an electrical signal at the output IDT. SAW devices based on ZnO and V-doped ZnO films were designed and fabricated. Frequency response of SAW devices is measured. In addition, finite element simulations of SAW devices are shown to be in agreement with measurement results. We discuss resonance frequency and insertion loss of SAW devices.

Keywords: Piezoelectric, thin films, SAW, ZnO.

ÖZET

ÇİNKO OKSİT TABANLI YÜZEY AKUSTİK DALGA AYGITLARININ DENEYSEL VE HESAPLAMALI OLARAK GELİŞTİRİLMESİ

Elif Özgöztaşı
Malzeme Bilimi ve Nanoteknoloji Bölümü, Yüksek Lisans
Tez Yöneticisi: Assist. Prof. Dr. Ali Kemal Okyay
Eylül, 2014

Piezoelektrik malzemeler mikrofonlar, ivmeölçerler, hoparlörler, hidrofonlar, basınç sensörleri gibi farklı dönüştürücü tiplerinde kullanılmaktadır. İnce film piezoelektrik malzemeler geleneksel büyük piezoelektrik seramiklerle karşılaştırıldığında CMOS teknolojisi ile entegre cihazlar geliştirilmesi açısından umut vericidir. Bu ince filmlerin arasında, çinko oksit (ZnO) vanadyum (V) ile katkılandığında çok büyük piezoelektrik etki göstermesi sebebiyle ilgi çekicidir.

Bu çalışmada ZnO ile V-katkılı ZnO ince filmlerin kaplanması geliştirilmiştir. ZnO ince filmlerin malzeme karakterizasyonu gerçekleştirilmiştir. Aynı zamanda ZnO temelli yüzey akustik dalga (SAW) aygıtları geliştirilmiştir. SAW aygıtları giriş ve çıkış olmak üzere birbirine geçen dönüştürücü (IDT) çiftlerinden oluşur. Değişen elektrik alan giriş IDT den uygulandığında piezoelektrik ince filmin yüzeyinde yüzey akustik dalgaları oluşturur ve bu dalgalar çıkış IDT de tekrar elektriksel sinyale dönüştürülür. ZnO ve V-katkılı ZnO temelli SAW aygıtları dizayn edilmiş ve üretilmiştir. SAW aygıtlarının frekans cevapları ölçülmüştür. Buna ek olarak, sonlu eleman yöntemi kullanılarak SAW aygıtlarının simulasyonları yapılmış ve simulasyon sonuçları ölçüm sonuçlar ile tutarlılık göstermiştir. SAW aygıtlarının rezonans frekansları ve geçiş kayıpları tartışılmıştır.

Anahtar sözcükler: Piezoelektrik, ince filmler, SAW, ZnO.

Acknowledgement

From the beginning of my education life, I know very special friends and academicians to this point. I would like to express my deepest and very special thanks to these people.

Firstly, I would like to express my gratitude to my supervisor Dr. Ali Kemal Okyay, for his invaluable support, kindness and his beliefs about my success sometimes even more than me. I would like to thank to him also for his encouragement and guidance. I am thankful to him for teaching me how can I survive in the academic world. I am grateful to him for his support about my Ph.D in EEE department.

I would like to thank my thesis committee members Prof. Dr. Ceyhun Bulutay and Dr. Necmi Bıyıklı for their valuable comments and suggestions about this thesis.

I am deeply grateful to Prof Dr. Ceyhun Bulutay for his teaching skills when I was in Physics Department and he always inspires me. I am very thankful to him for priceless guidance and his time.

I would like to thank Dr. Kağan Topallı, he never refrains from helping with our unsolvable problems, he enlightens me about not only technical subjects but also life matters. His joining to UNAM is priceless for us.

I would like to thank UNAM staff, Semih Yaşar, Fikret Piri, Abdullah Kafadenk for their help in the cleanroom and equipments.

I would like to thank Okyay group members, Fatih Bilge Atar, Furkan Çimen, Sami Bolat, Berk Berkan Turgut, Burak Tekcan, Muhammed Maiz Ghauri, Amin Nazirzadeh, Yunus Emre Kesim, Gamze Ulusoy, Amir Ghobadi, Dr. Sabri Alkış, Dr. Kinyas Polat, Abdullah Gök and Levent Erdal Aygun. I am also thankful to my past and present office friends, Pelin Kübra İşgör, Merve Marçalı, Canan Kurşungöz, Seda Kizir and Hamit Eren.

I am deeply thankful to my Arabic instructor, Dr. Ahmet Beyatlı, I can not express his priceless effect on my studies with words, he is a very special instructor in my life. His kindness and guidance are invaluable for me all through my life.

I would like to thank my precious friends who make my life better, more enjoyable and sweeten. Now we are living different lives, but you are very important for my life and afterlife. I am thankful to Merve Akgül for every moment of our friendship. I would like to thank my friend Reyhan Yılmaz for our friendship. I am thankful to 'the new moms' Mümine Dönmez and Feyza Bozkurt, their friendship and now their babies 'Hira' and 'Fatih' are the beauties of my life.

I would like to thank Şeyma Canik, for her generous, warm, enjoyable and colorful friendship. Our paths are not separated from the freshman year in the Physics Department.

I am thankful to my lovely friend Ayşe Özcan, she always opens the doors of new worlds with her ideas. Her existence in my life is priceless. She is always more than a friend for me.

No words would express my deepest thanks to my wonderful family, my parents Ayşe Deniz and Mehmet, my elder brother Mustafa and my lovely sisters Ayşenur and Şeyma. My parents are my privilage in this world and I know that they always stand behind me.

Finally, my deepest gratitude goes to my dear husband Muhammed, I cannot complete these works without his endless supports, helps, patience and love. No word is enough to express my thanks to him only I can say that without him everything would be meaningless.

To my beloved parents, Ayşe Deniz and Mehmet...

Contents

List of Figures

List of Tables

Chapter 1

Introduction

Piezoelectric thin films are used in diverse fields with different types of transducers. Beyond the traditional piezoelectric materials, zinc oxide (ZnO) is attractive due to the giant piezoelectric effect when doped with vanadium for the piezoelectric applications. In this thesis, we investigate the surface acoustic wave (SAW) devices as a piezoelectric application of ZnO. We simulated resonance frequency and insertion loss of SAW devices which are based on ZnO. In addition to simulations, ZnO and V-doped ZnO SAW devices were fabricated and characterized for their promising piezoelectric properties. SAW devices are formed from a pair of the interdigitated transducers (IDT). One of them is input IDT and the other is the output IDT. IDTs are fabricated on the piezoelectric thin film. Applied oscillating electric field from input IDT can create surface acoustic waves in the piezoelectric thin film and these acoustic waves can be converted into electrical signal again at the output IDT. According to the properties of IDTs finger width, finger spacing, number of fingers, the space between the IDTs etc. and the properties of piezoelectric layer, device performance is determined in terms of resonant frequency and insertion loss.

1.1 Historical Overview of Piezoelectric Effect and Piezoelectric Materials

From a historical perspective, the piezoelectric effect is discovered by French physicists Curie brothers in 1880 [5]. They found that certain materials accumulate surface charges when they were stressed mechanically such as tourmaline, quartz, topaz, cane sugar and Rochelle salt. Curie brothers observed only the direct piezoelectric effect. The converse piezoelectric effect was estimated from the fundamental laws of thermodynamics by Lippmann [6]. The first utilization of piezoelectric effect in sensors is reported during the World War I. The doctoral student of Curie brothers, Paul Langevin developed an ultrasonic submarine detector [7]. This detector was made of thin quartz crystals with the resonant frequency 50 KHz [7]. In the period of World War II, scientists worked on improvement of piezoelectric materials [8]. They discovered certain ceramic materials which exhibited 100 times higher dielectric constants than powders [8]. These ceramics were used in a wide variety of piezoelectric applications. In 1945, the mixed oxide compound barium titanate was found which has easy production and shaping and piezoelectric coefficient higher than natural materials by an electrical poling process [8]. After this discovery, the mixed oxide materials attracted attention the focus of researchers. By using these materials, many piezoelectric devices are investigated such as mechanical frequency filters, surface acoustic wave devices bulk acoustic wave devices, microphones, speakers, hydrophones, accelerometers, pressure sensors, etc [8]. The well known and used piezoelectric materials are lead zirconate titanate, barium titanate and quartz up to date. The non-semiconductive nature of these materials limits their use in todays MEMS, electronic, optic applications [9]. Recently, semiconducting piezoelectric materials are being investigated into by researchers because of their piezoelectric and semiconducting properties which can be used in similar devices or hybrid applications [9]. The piezoelectric semiconducting materials ZnO, GaN, AlN, InN come from wurtzite non-Centro symmetrical crystal family.

1.2 Thesis Overview

In this thesis, we investigate ZnO based SAW devices from two points of view. In Chapter 2, piezoelectric effect and piezoelectric materials introduced due to their indispensable nature for the SAW device applications. This is followed by a brief introduction to the SAW devices. In Chapter 3, the results of the FEM simulations are demonstrated. In Chapter 4, we report the material characterization of ZnO and V-doped ZnO films, fabrication of SAW devices, measurement setup with network analyzer and the device characterization results. Chapter 5 completes this thesis by concluding remarks.

Chapter 2

Theory of Piezoelectricity and Surface Acoustic Wave Devices

Piezoelectricity and piezoelectric materials are indispensable for the SAW devices. To understand the mechanism of the SAW device first theory of piezoelectric effect and properties of the piezoelectric materials are discussed. In this chapter, piezoelectric effect and materials are introduced followed by SAW fundamentals.

2.1 Piezoelectric Effect

The piezoelectric effect can be defined as converting mechanical stress and electrical energy to each other. The word piezo derives from Greek Language, which means to to press. The conversion of mechanical energy to the electrical energy is the direct piezoelectric effect. The indirect piezoelectric effect is defined as an applied electric field creates mechanical deformation inside the material.

One of the concepts important to understanding the piezoelectric effect is electric polarization and dielectric materials. When a material is perturbed with an external electric field, it adapts to this perturbation by reorienting the positions of positive and negative charges. Dipoles are created as a result of this process.

The formation of dipoles under the electric field is defined as polarization. Three main types of polarization can exist in the materials: electronic, ionic and orientation. In electronic polarization, under the influence of the electric field the center of the negatively charged electron cloud displace relative to the positive nucleus of the atom. Ionic polarization is the movement of anions and cations in opposite direction by the influence of the electric field. The last type is orientation polarization which is observed in the materials which have permanent dipoles. In this type of polarization, permanent dipoles align according to the direction of the applied electric field. The total electric polarization of the material is the summation of the different types of polarizations inside the material. The net polarization is formed by N electric dipoles and can be expressed as:

$$\vec{P} = \frac{1}{V} \sum_{k=0}^{N} \vec{p_k} \tag{2.1}$$

A dielectric material can be defined after understanding the polarization. Although dielectric materials are electrically insulating, they have electric dipole structure and at least one of the polarization type can be observed typically under the influence of electric field.

Now we can move to piezoelectric materials. Piezoelectric materials are dielectric materials which exhibit polarization phenomenon in the presence of the mechanical stress in addition to electric field. If there is no external force or electric field the material is in equilibrium and electrically neutral. This can be seen in Figure 2.1(a). When a mechanical stress is applied to the piezoelectric material, lattice can be deformed and this causes the creation of dipoles as shown in Figure 2.1(b). The overall effect of each polarization is fixed charges on the surface of the material as indicated in the Figure 2.1(c).

The piezoelectric effect can be expressed with the elastic and dielectric coupled equations. In these equations elastic parameters are strain S and stress T, dielectric parameters are electric field E and electric charge density displacement field D. The piezoelectric materials have linear response at low mechanical loads

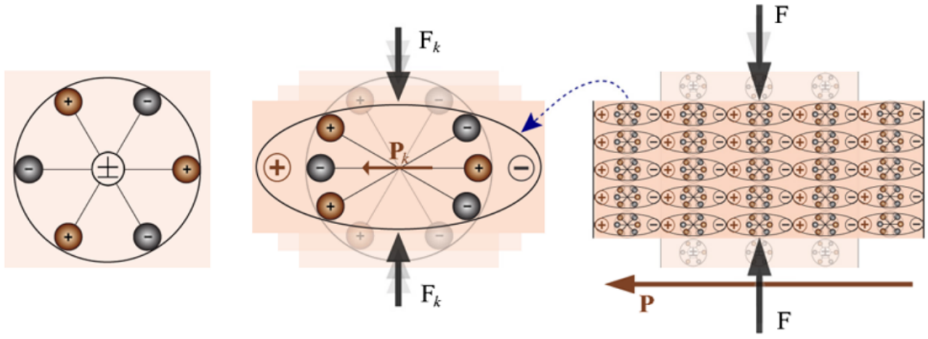

Figure 2.1: Illustration of piezoelectric effect (a) molecule with no external force (b) molecule in the precence of external force (c) the polarization effect in the piezoelectric material

and at low electric fields. By using linear theory of the piezoelectric effect, polarization of material can be expressed in terms of applied stress on the material as in Equation 2.2 where P_p is the polarization which is the result of piezoelectric effect (the subscript p denotes effects which are created by piezoelectric effect). T is the mechanical stress and d is the piezoelectric coefficient, which express the linear relation between the electrical and mechanical effects.

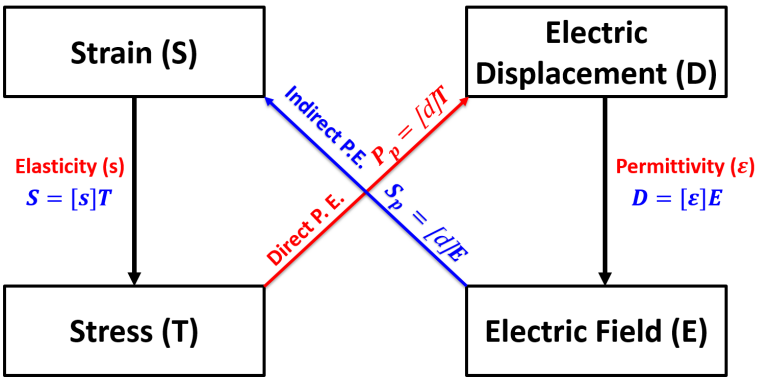

Figure 2.2: Piezoelectric relation between mechanical and electrical parameters

$$P_p = dT \tag{2.2}$$

$$S_p = dE \tag{2.3}$$

The indirect piezoelectric effect can be expressed mathematically in the Equation 2.3 where S_p is the strain which is produced by the indirect piezoelectric

effect. E is the applied electric field. The piezoelectric linear constitutive relations are combination of electric displacement field equations and Hookes Law. The electric displacement field equation is given by Equation 2.4, ε denotes the permittivity of the material. Hooke's law is formulated in Equation 2.5 where s is the elastic compliance of the material.

$$D = \varepsilon E \tag{2.4}$$

$$S = sT \tag{2.5}$$

Before moving to the piezoelectric constitutive relations, tensor directions are introduced in Figure 2.3. 1 corresponds to x, 2 denotes y and 3 expresses z directions, 4,5,6 are the shear planes of these directions respectively. By the linear piezoelectric theory, the coupling between stress, strain, electric field and electric displacement can be formulated with the tensor notation in Equation 2.6 and 2.7.

$$S_i = s_{ij}^E T_j + d_{ik} E_k \tag{2.6}$$

$$D_l = d_{lj} T_j + \varepsilon_{lk}^T E_k \tag{2.7}$$

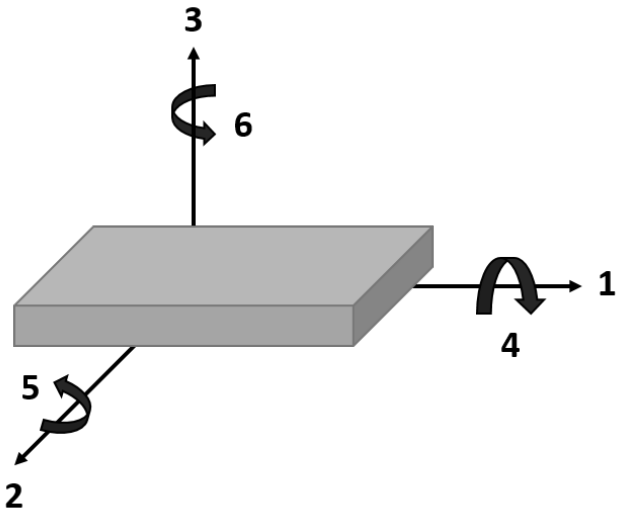

Figure 2.3: Axis nomenclature

In Equation 2.6 and 2.7, S_i is a strain tensor in the direction i, s_{ij}^E is an elastic compliance tensor and superscript E denotes the constant electric field, T_j is a stress in the direction j, d_{ik} is an indirect piezoelectric constant tensor under an applied electric field E_k from the direction k. D_l is the electric displacement in the direction l. d_{lj} is the direct piezoelectric constant tensor under the applied mechanical stress T_j from the direction j. ε_{lk}^T denotes the dielectric constant tensor under constant stress. Using the directions shown in Figure 2.3, electromechanical equations can be written in the matrix form as in Equation 2.8 and 2.9 . We can apply the electric field from the direction 1,2 and 3 but mechanical stress and strain can be applied or generated from the directions 1, 2, 3, 4, 5 and 6.

$$\begin{pmatrix} S_1 \\ S_2 \\ S_3 \\ S_4 \\ S_5 \\ S_6 \end{pmatrix} = \begin{pmatrix} s_{11}^E & s_{12}^E & s_{13}^E & s_{14}^E & s_{15}^E & s_{16}^E \\ s_{21}^E & s_{22}^E & s_{23}^E & s_{24}^E & s_{25}^E & s_{26}^E \\ s_{31}^E & s_{32}^E & s_{33}^E & s_{34}^E & s_{35}^E & s_{36}^E \\ s_{41}^E & s_{42}^E & s_{43}^E & s_{44}^E & s_{45}^E & s_{46}^E \\ s_{51}^E & s_{52}^E & s_{53}^E & s_{54}^E & s_{55}^E & s_{56}^E \\ s_{61}^E & s_{62}^E & s_{63}^E & s_{64}^E & s_{65}^E & s_{66}^E \end{pmatrix} \begin{pmatrix} T_1 \\ T_2 \\ T_3 \\ T_4 \\ T_5 \\ T_6 \end{pmatrix} + \begin{pmatrix} d_{11} & d_{12} & d_{13} \\ d_{21} & d_{22} & d_{23} \\ d_{31} & d_{32} & d_{33} \\ d_{41} & d_{42} & d_{43} \\ d_{51} & d_{52} & d_{53} \\ d_{61} & d_{62} & d_{63} \end{pmatrix} \begin{pmatrix} E_1 \\ E_2 \\ E_3 \end{pmatrix} \quad (2.8)$$

$$\begin{pmatrix} D_1 \\ D_2 \\ D_3 \end{pmatrix} = \begin{pmatrix} d_{11} & d_{12} & d_{13} & d_{14} & d_{15} & d_{16} \\ d_{21} & d_{22} & d_{23} & d_{24} & d_{25} & d_{26} \\ d_{31} & d_{32} & d_{33} & d_{34} & d_{35} & d_{36} \end{pmatrix} \begin{pmatrix} T_1 \\ T_2 \\ T_3 \\ T_4 \\ T_5 \\ T_6 \end{pmatrix} + \begin{pmatrix} \varepsilon_{11}^T & \varepsilon_{12}^T & \varepsilon_{13}^T \\ \varepsilon_{21}^T & \varepsilon_{22}^T & \varepsilon_{23}^T \\ \varepsilon_{31}^T & \varepsilon_{32}^T & \varepsilon_{33}^T \end{pmatrix} \begin{pmatrix} E_1 \\ E_2 \\ E_3 \end{pmatrix} \quad (2.9)$$

According to crystal symmetry of the wurtzite materials like ZnO, AlN which are the interest of this thesis, electromechanical tensor some matrix elements of the electromechanical tensor are equal to zero and the resulting matrices are given in the Equation 2.10 and 2.11.

$$\begin{pmatrix} S_1 \\ S_2 \\ S_3 \\ S_4 \\ S_5 \\ S_6 \end{pmatrix} = \begin{pmatrix} s_{11}^E & s_{12}^E & s_{13}^E & 0 & 0 & 0 \\ s_{21}^E & s_{22}^E & s_{23}^E & 0 & 0 & 0 \\ s_{31}^E & s_{32}^E & s_{33}^E & 0 & 0 & 0 \\ 0 & 0 & 0 & s_{44}^E & 0 & 0 \\ 0 & 0 & 0 & s_{55}^E & & \\ 0 & 0 & 0 & 0 & 0 & s_{66}^E \end{pmatrix} \begin{pmatrix} T_1 \\ T_2 \\ T_3 \\ T_4 \\ T_5 \\ T_6 \end{pmatrix} + \begin{pmatrix} 0 & 0 & d_{13} \\ 0 & 0 & d_{32} \\ 0 & 0 & d_{33} \\ & d_{24} & 0 \\ d_{15} & 0 & 0 \\ 0 & 0 & 0 \end{pmatrix} \begin{pmatrix} E_1 \\ E_2 \\ E_3 \end{pmatrix} \quad (2.10)$$

$$\begin{pmatrix} D_1 \\ D_2 \\ D_3 \end{pmatrix} = \begin{pmatrix} 0 & 0 & 0 & 0 & d_{15} & 0 \\ 0 & 0 & 0 & d_{24} & 0 & 0 \\ d_{31} & d_{32} & d_{33} & 0 & 0 & 0 \end{pmatrix} \begin{pmatrix} T_1 \\ T_2 \\ T_3 \\ T_4 \\ T_5 \\ T_6 \end{pmatrix} + \begin{pmatrix} \varepsilon_{11}^T & 0 & 0 \\ 0 & \varepsilon_{22}^T & 0 \\ 0 & 0 & \varepsilon_{33}^T \end{pmatrix} \begin{pmatrix} E_1 \\ E_2 \\ E_3 \end{pmatrix} \quad (2.11)$$

In this chapter, piezoelectric effect fundamentals are briefly introduced. The piezoelectric effect and elastic constants are important for the evaluation of the piezoelectric device response.

2.2 Piezoelectric Materials

Piezoelectric materials have unbalanced charge distribution in their unit cell due to the noncentrocymetric lattice structure. This lattice structure can be found in different types of crystals, Perovskite and Wurtzite are the most common types of noncentrosymetric crystals [10]. In the perovskite structure, there are two metal cation and an oxygen anion. At room temperature, the negatively charged oxygen atom repels the positively charged sublattices of metal atoms and the polarization is occurring in the lattice. One of the perovskite structure compounds is the Barium Titanate. It has two phases cubic and tetragonal. It shows piezoelectricity when it is in the tetragonal phase. In Figure 2.4, its cubic (a) and tetragonal phases (b, c) are illustrated [1]. The lattice structure of

Wurtzite materials is hexagonal closed packed (HCP) structure which is shown in Figure 2.5. ZnO, AlN, ZnS, GaN and BN, etc. are in the Wurtzite structure. These materials are semiconductors and they are promising materials in the area of piezoelectric and semiconducting coupled applications.

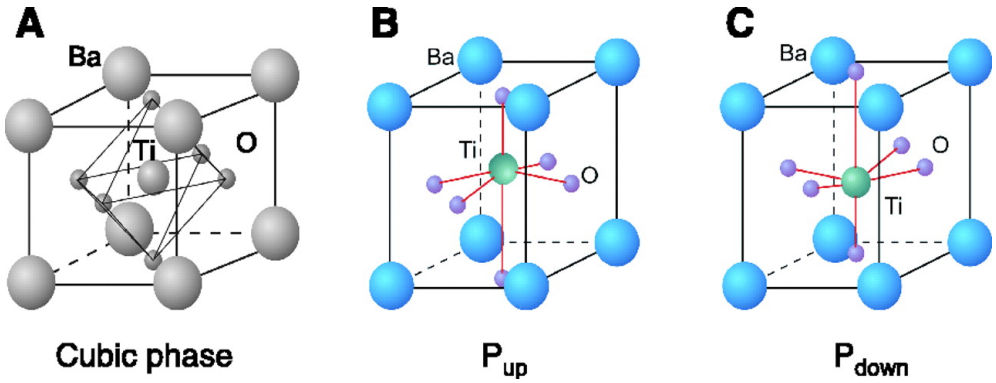

Figure 2.4: The crystal lattice structure of Barium Titanate (a) cubic phase at high temperatures (b) tetragonal phase at room temperature with up polarization vector (c) tetragonal phase at room temperature with down polarization vector

Figure 2.5: Wurtzite crystal unit cell

One of the important limitations in piezoelectric materials is Curie point, T_c, which is the temperature that many piezoelectric materials lose their polarizability above T_c because they go to the paraelectric centrosymmetric phase. The Curie temperature is valid for special ferroelectric class of piezoelectric materials and they exhibit dramatically high piezoelectric coefficient in the vicinity of the Curie point [11]. This is the advantage of the high Curie point piezoelectric materials. The promising semiconducting-piezoelectric materials ZnO, AlN are not ferroelectric. Thus, their piezoelectric properties do not depend on the Curie

Table 2.1: Comparision of the properties of ZnO, AlN and PZT [3]

	ZnO	AlN	PZT
Density(kg/m^3)	5610	3230	7570
Piezoelectric costant d_{33} (pC/N)	11.67	5.49	374
Young Modulus (GPa)	201	308	68
Index of refraction	2.01	2.08	2.4
Band Gap (eV)	3.4	6.2	2.67

point. They still have an operating temperature problem, but this temperature is higher than the Curie point of the traditional piezoelectric ceramic. Due to the properties such as the wide operating temperature range and high Young modulus, etc. these materials are becoming advantageous in the piezoelectric device applications. In Table 2.1 some properties of ZnO, AlN and PZT are compared.

Zinc oxide and aluminium nitride have several advantages over lead zirconate titanate. First of all, ZnO and AlN are compatible materials with the today's MEMS technology with their easier deposition and good crystallinity. They have a wide band gap, high breakdown field and high dielectric constant [3]. Besides all, their acoustic velocity is higher than many piezoelectric materials, thus they are good candidate for the surface acoustic wave device applications [3].

2.2.1 Zinc Oxide and Vanadium Doped Zinc Oxide

For surface acoustic wave devices and other piezoelectric applications, desirable properties of ZnO thin films are high crystal quality, good stoichiometry, low roughness, low acoustic loss, good thermal stability, easy deposition, low film stress and compatibility with MEMS and CMOS technology [12]. Many different deposition methods for ZnO are reported that includes sputtering, atomic layer deposition, metal-organic chemical vapor deposition and pulsed layer deposition [12]. We use radio-frequency magnetron reactive sputtering method due to the good film texture and easier production. RF sputtering parameters, which affect the film quality and piezoelectric and acoustic properties, are RF-power, substrate temperature, sputtering gas pressure, O_2/Ar gas ratio. According to the literature, low gas pressure makes a fine grain film, higher plasma power increase the

deposition rate, but increase the surface roughness at the same time, the gas ratio determines the stoichiometry of the ZnO films, the sputtered ZnO films exhibits the piezoelectric effect without post-poling process [13]. The ZnO crystalline structure is Wurtzite structure and the preferred orientation is (0001) plane (Figure 2.6) for the piezoelectric applications. The (0001) plane is the lowest surface free energy plane, if there is no external energy source and under equilibrium conditions ZnO films grow along the (0001) direction [14]. It has been reported that the other orientation peaks become to appear as the film thickness increases [15]. The acoustic velocity is the most important property for specifying the surface acoustic wave device operating frequency. The acoustic velocity of the ZnO highly depends on the film thickness, substrate material. If the substrate material acoustic velocity is high, ZnO acoustic velocity increases. In Table 2.2, the substrate dependent property change of ZnO is summarized [4, 16, 17]. Among them, the best substrate materials are AlN and diamond for the higher acoustic velocity of ZnO to higher frequency applications. The film thickness dependence of acoustic velocity and operating frequency are reported. Increase in thickness results in low acoustic velocity is reported [18]. Therefore the phase velocity of the acoustic wave can vary between ZnO and substrate acoustic velocities [18]. Below 1 μm ZnO layer can not show surface acoustic wave resonant modes are reported [18].

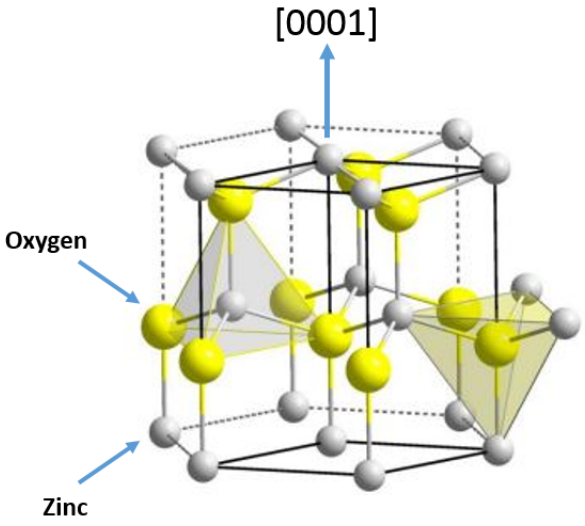

Figure 2.6: Wurtzite crystal structure

Table 2.2: Comparision of ZnO velocities and thermal expansion coefficient (TEC) for different substrate materials [4]

Device Type	**Substrate Materials**	**Structure**	**v(m/s)**	**TEC** ($10^{-6}K^{-1}$)
ZnO	ZnO	HCP	2724	2.9
ZnO/Si	Si(111)	Cubic	2653	3
ZnO/Pt	Pt(111)	Cubic	2684	8.8
ZnO/Au	Au(111)	Cubic		14
ZnO/sapphire	Sapphire(0001)	HCP		8.4
ZnO/AlN	AlN	HCP	4522	5.3
ZnO/diamond	Diamond(111)	Cubic	10000-12000	1.18
ZnO/AlN/diamond	ZnO/AlN/diamond		12200	1.18

A diluted magnetic semiconductor (DMS) is obtained by doping a non-magnetic semiconductor with transition metal (TM) elements (Ti, V, Cr, Mn, Fe, Co, Ni, Cu, etc.) [19]. A low magnetic curie point problem for the practical applications of DMSs are reported [20, 21]. The reported information about DMSs in 2000 is that T_c could be increased in DMSs and ferromagnetism was stable in wide band gap semiconductors (ZnO, GaN, etc.) [22]. These ferromagnetic properties of TM doped ZnO has been investigated in detail in the literature, recently ferroelectricity has been discovered in these doped materials. Yang et al.[23, 24], reported that V and Cr doped ZnO exhibit 10 times higher piezoelectric coefficient d_{33} than the pure ZnO [24]. They use co-sputtering method for doping process, obtain a series of V-doped ZnO samples, the highest piezoelectric coefficient ($d_{33} = 110pC/N$) is observed in the 2.5% V doped ZnO samples. The reason of this increase was discussed in two perspectives. The first one is the increasing crystal quality of ZnO films by V-doping, however, both doped and undoped samples XRD results shows the highly oriented films and this effect is limited on the piezoelectric properties. The secondly, they discussed the intrinsic factors like the emergence of switchable spontaneous polarization due to the V doping. In this study, we tried to fabricate low insertion loss SAW devices by using V-doped ZnO thin films.

2.3 Surface Acoustic Wave Devices

To understand the surface acoustic waves in a solid, first wave propagation in an elastic medium should be understood. In this part, wave propagation in an elastic medium fundamentals is introduced. These are coupled with piezoelectric equations in Chapter 2.1 and the wave propagation in a piezoelectric medium equation is obtained. Finally, surface acoustic wave propagation in a piezoelectric medium is defined.

2.3.1 Fundamentals of Surface Acoustic Wave Theory

An elastic media behavior can be defined as a mass-spring system in which disturbance of a single element results in the propagation of this disturbance in the medium. There is a difference between the free surface particles and the interior particles due to the free surface particles have a boundary from only one side. As a result of these boundary conditions, unique modes of wave propagation can only exist on a free surface of a medium. First, plane waves in an elastic medium are examined. An elastic wave result from the combination of distributed elastic and inertial forces [25]. The waves in a solid depend on both the boundaries of the solid and its properties [25]. In Figure 2.7, bulk longitudinal, bulk transverse and surface (Rayleigh) waves are illustrated.

As a result of solid deformation, each particle changes their original position and this change is expressed with the displacement vector u (x, y, z, t). The displacements which are generated from a plane wave, is in the direction of propagation. If the plane wave direction of propagation is in the x direction, the displacement vector becomes as in Equation 2.12 where the u_1, u_2, u_3 are particle displacement in the x, y, and z directions. ω is the angular frequency of the wave which equals to $2\pi f$. k is the wave number which equals to $2\pi/\lambda$.

$$\mathbf{u}(x, y, z, t) = (u_1\mathbf{x} + u_2\mathbf{y} + u_3\mathbf{z})e^{j(\omega t - kx)} \tag{2.12}$$

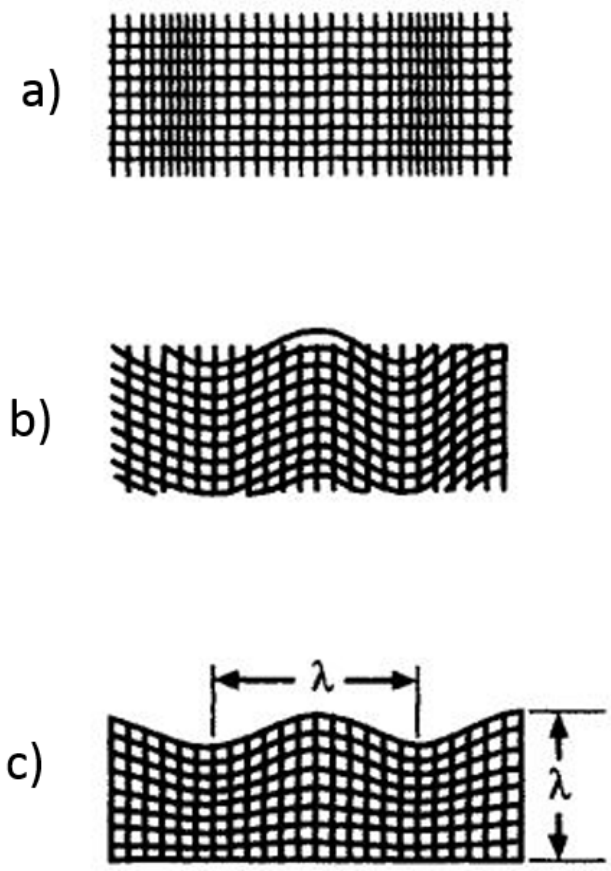

Figure 2.7: Elastic waves in a solid (a) bulk longitudinal (compressional) waves (b) bulk transverse (shear) waves (c) surface (Rayleigh) waves

The local deformations in a solid are expressed with the displacement gradient ∇u which is the second-rank tensor. The gradient matrix is expressed in Equation 2.13.

$$\nabla u = \begin{pmatrix} \frac{\partial u_1}{\partial x} & \frac{\partial u_1}{\partial y} & \frac{\partial u_1}{\partial z} \\ \frac{\partial u_2}{\partial x} & \frac{\partial u_2}{\partial y} & \frac{\partial u_2}{\partial z} \\ \frac{\partial u_3}{\partial x} & \frac{\partial u_3}{\partial y} & \frac{\partial u_3}{\partial z} \end{pmatrix} \tag{2.13}$$

When the gradient of displacement vector and its transpose is added, the result gives the strain matrix $\mathbf{S}$ in Equation 2.14. Strain is the dimensionless ratio of the stressed length of the material to its unstressed length. Stress is the force which is applied to the unit area of the material.

$$S_{ij} = \frac{1}{2}(\partial u_i/\partial x_j + \partial u_j/\partial x_i) \tag{2.14}$$

The stress tensor **T** is used to define the state of stress at each point in a solid. The equation of motion for elastic deformations in a solid (particularly wave motion) is derived from the definitions of stress and strain. By considering the forces acting on the only x direction of the cube is expressed as in Equation 2.15

$$F_1 = [(T_{11}+\Delta T_{11})A_1 - T_{11}A_1] + [(T_{12}+\Delta T_{12})A_2 - T_{12}A_2] + [(T_{13}+\Delta T_{13})A_3 - T_{13}A_3] \tag{2.15}$$

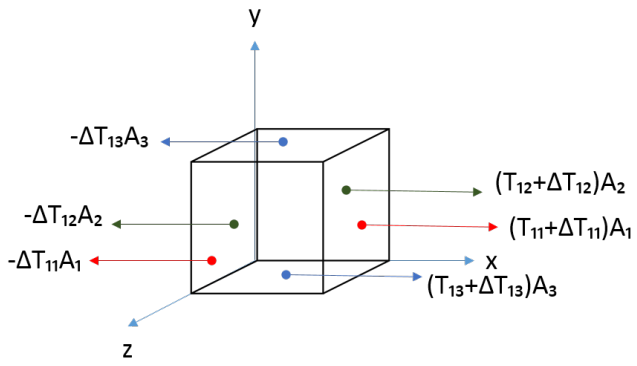

Figure 2.8: The x-directed forces acting on each face of the cube

From Newton's law, $F = m\ddot{\mathbf{u}}$, $\ddot{u} = \partial^2 u_i/\partial t^2$, the mass of the unit volume equals to $\rho\Delta x\Delta y\Delta z$, where ρ is the density of the material. By using Equation 2.15 in Newton's law and dividing by the volume we can obtain the equation of motion in one-dimension. And this can be generalized for all directions and expressed as in Equation 2.16.

$$\sum_{j=1}^{3} \frac{\partial T_{ij}}{\partial x_j} = \rho \frac{\partial^2 u_i}{\partial t^2} \tag{2.16}$$

Stress and strain tensors have a linear relation as expressed in Equation 2.5 and they are symmetric and because of that we can reduce the indices, two to

one by 11 - 1, 22 - 2, 33 - 3, 23 or 32 - 4, 13 or 31 - 5, 12 or 21 - 6. These give the reduced elastic constitutive relation which is given in Equation 2.17.

$$T_j = \sum_{j=1}^{6} c_{ij} S_j \tag{2.17}$$

From this point, the wave equation of the non-piezoelectric elastic solid can be defined by differentiating the Equation 2.17 and equate the right hand side of it with the right hand side of Equation 2.16.

$$\rho \frac{\partial^2 u_i}{\partial t^2} = \sum_{j,k,l=1}^{3} c_{ijkl} \frac{\partial^2 u_k}{\partial x_j \partial x_l} \tag{2.18}$$

From the piezoelectric constitutive relations which are examined in Chapter 2.1, the wave equation of piezoelectric solid can be determined. In piezoelectric wave equation displacements are coupled with the electric potential ϕ which is $E_k = -\partial\phi/\partial x_k$.

$$T_{ij} = \sum_{k,l=1}^{3} c_{ijkl} \frac{\partial u_l}{\partial x_k} + \sum_{k=1}^{3} e_{ijk} \frac{\partial \phi}{\partial x_k} \tag{2.19}$$

The wave equation for the piezoelectric elastic solid is written by the same calculation steps of the equation of motion of the non-piezoelectric elastic solid. Taking the derivative of Equation 2.19 and applying the equation of motion in Equation 2.18 the piezoelectric wave equation is defined in Equation 2.20.

$$\rho \frac{\partial^2 u_i}{\partial t^2} = \sum_{j,k,l=1}^{3} c_{ijkl} \frac{\partial^2 u_l}{\partial x_k \partial x_j} + \sum_{j,k=1}^{3} e_{ijk} \frac{\partial^2 \phi}{\partial x_k \partial x_j} \tag{2.20}$$

The difference between the non-piezoelectric and piezoelectric solids wave function is the additional potential term which defines the generation of an acoustic wave by an applied, time varying electric-field. The wave motions create an electric potential and this results in that piezoelectric acoustic wave can be detected electrically.

Acoustic wave sensor devices based on piezoelectric materials transduce the acoustic and electrical energies to each other. Surface acoustic wave devices are one type of acoustic sensors in which the acoustic waves are generated at the crystal surface with unique modes. These waves were discovered by Rayleigh in 1887. Rayleigh wave provides the confinement of energy in the surface which can be excited or collected by the surface electrodes in the piezoelectric materials. These waves are very sensitive to surface perturbations which allows the use of surface acoustic wave devices as a sensing element. Shear and compressional waves are combined and propagate together at the surface of a solid, device normal direction forces are zero. A surface acoustic wave with propagation direction z, and displacement is u(y) is expressed as in Equation 2.21. It is the displacement component and $u_i(y)$ changes as $e^{2\pi y/\lambda}$, where λ is the wavelength of the SAW and y is the depth into the substrate. Much of the energy is distributed within one wavelength into the substrate. When acoustic energy is confined closer to the surface, sensitivity of the surface perturbations is increased.

$$u(x,y,z,t) = (u_x(y)e^{j\phi_1}\hat{x} + u_y(y)e^{j\phi_2}\hat{y} + u_z(y)e^{j\phi_3}\hat{z})e^{j\omega-\gamma_z} \tag{2.21}$$

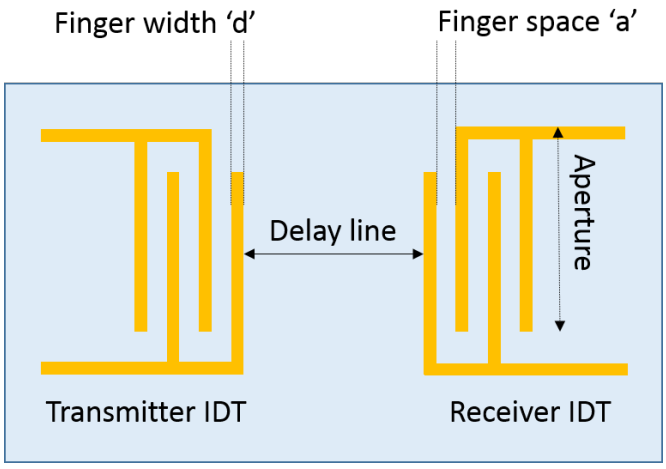

Figure 2.9: Geometrical parameters of typical SAW device

The first SAW device with the interdigital electrodes were demonstrated by R.M. White. SAW devices now are used in the widespread area of applications as filters, resonators, delay lines, convolvers, biosensing applications, microfluidics

applications. SAW excitation on the piezoelectric substrates are made with interdigital transducer (IDT), as shown in Figure 2.9 [25]. The most efficient device response is measured when the λ match with the transducer periodicity d for the constructive interference by $\lambda = 2(a + d)$ and equation 2.22 defines the center frequency of the SAW device.

$$f_0 = \frac{v_0}{\lambda} \tag{2.22}$$

where v_0 is the propagation velocity of SAW. A bandwidth of the device is determined by the number of IDT fingers, they are inversely proportional, if the number of fingers increase, bandwidth of the device becomes narrower. Delay line characterizes the phase shift of the SAW device, if the delay line becomes wider, the phase shift increases.

The electrical potential that is created by the applied continuous wave voltage V_1 to a finger has a simple transfer function as in the Equation 2.24(μ_s). ϕ^+ denotes that the SAW propagates right, ϕ^- denotes that the SAW propagates the left. The frequency response increase with the constructive interference of each finger response.

$$\phi^{\pm} = \mu_s V_1 \tag{2.23}$$

Equation 2.24 shows the only one finger response, if all fingers are excited in IDT, the wave potential can be written as the vector sum of each finger contributions:

$$\phi^+(z) = \mu_s \sum_{n=0}^{N_f-1} V_n e^{jk(z-z_n)} \tag{2.24}$$

z_n refers the position of n^{th} finger excited by voltage V_n. The frequency response of the SAW device is proportional with the Fourier transform of the sequence of the finger contributions.

Chapter 3

Computational Methods for Surface Acoustic Wave Device Applications

This chapter includes the simulation results of ZnO based SAW devices, according to different parameters which affect the SAW performance. Before the results are presented, the brief introduction of finite element model situlations and our simulation tool COMSOL Multiphysics is provided.

3.1 Introduction to Finite Element Method (FEM) Simulations

The finite element method (FEM) is a computational tool used to find approximate solutions to complex engineering problems. The necessity of FEM simulations emerges from the complex engineering structures and their complex mathematical solutions. In the FEM, there is a boundary value problem which is a

mathematical problem with the dependent variables which must satisfy the differential equation within the known independent variables of the system which is defined with the specific boundary conditions[26]. For FEM simulations, dependent variables, independent variables and boundary conditions must be well-defined. After defining the physical problem in the FEM simulations, the 'finite element' part of the simulation is taken into the consideration. FEM divide the modeled structure to several elements and reconnect these elements with the nodes. This process is called as meshing in the FEM simulations. Meshing is the approximation to the real physical model. After meshing, each node is solved by known dependent and independent variables and differential equations. It is important to note that FEM simulations do not produce absolute solutions. The meshing example is illustrated in Figure 3.1 [2]. The differential equations are solved for each node during the simulation and interpolation of solutions gives the entire solution of the physical system.

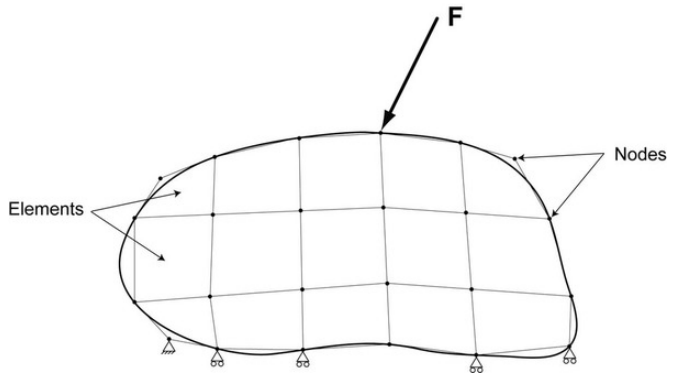

Figure 3.1: Illustration of elements and nodes in the meshed structure

Historically, Clough used the finite element term firstly in 1960 in the plane stress analysis [27]. During the 1960s and 1970s, the finite element method was used for applications in plate and shell bendings, pressure vessels, and general three-dimensional problems in elastic structures, uid ow and heat transfer [28, 29, 30, 31]. During 1960s, NASTRAN finite element code was developed by the United states for the space exploration program [32]. After these developments, many software packages for the finite element method simulations are introduced as ANSYS, ALGOR, COSMOS/M and COMSOL Multiphysics [33, 34, 35, 36].

3.2 Literature Summary of FEM Based SAW Simulations

In 1995 the first FEM analysis of the surface acoustic wave devices was implemented by Endoh [37]. The first SAW modeling with COMSOL was demonstrated by Nemade et al. in 2006 [38]. They modeled the one port SAW resonator. Lithium Niobate is the piezoelectric layer in their simulations, the frequency analysis of the SAW device is illustrated with the periodic boundary conditions.

In literature, eigenfrequency, frequency sweep and time domain analysis are used typically for the COMSOL simulations [39, 40, 41, 42, 43, 44, 45, 46]. In this thesis, we use eigenfrequency and frequency sweep and parametric sweep analysis simulate ZnO/SiO_2/Si SAW devices. We investigate the fundamental modes of ZnO/SiO_2/Si SAW devices and the effect of parameters as finger width, delay line, ZnO thickness, substrate thickness on the device frequency response.

3.3 2D ZnO SAW simulations

2D SAW simulations were performed in COMSOL 4.4. Eigenfrequency analysis is performed with two identical fingers and periodic conditions to find the fundamental modes of the SAW device and observe the displacement with applied voltage. In the frequency domain analysis, SAW devices were simulated in the frequency range that includes the fundamental mode, which is found in eigenfrequency analysis, with precise values of finger width, finger space, number of fingers and delay line. Perfectly matched layers were used to avoid the reflections of waves from boundaries. In a frequency sweep analysis study, insertion losses were calculated by exporting data to MATLAB. The parameters which affect the SAW device performance are described in the Chapter 2 as film thickness, substrate thickness, finger geometry and delay line length. These parameters are used in a parameter sweep study to demonstrate the effects on SAW performance. In all studies, we use the COMSOL Piezoelectric Devices Model.

3.3.1 Eigenfrequency Analysis

IDTs used in SAW sensors have many identical fingers. Simulation of the real devices has a high computational cost. In eigenfrequency analysis, an identical cell of the finger geometry of the SAW device is solved as shown in Figure 3.2 The substrate material is SiO_2/Si, the piezoelectric material is ZnO, finger width is 5μm and finger space is 5μm, ZnO thickness is chosen as 1μm, the substrate thickness is 80μm in order avoid bulk wave scatterings from the boundary conditions. Left and right sides of the structure shown in Figure 3.2 are defined as a periodic boundary condition in the model. The bottom side of the structure is fixed constraint. We set the electric potential for each finger +1V and -1V respectively. Eigenfrequency solution gives the modes of the structure and their corresponding frequencies at this boundary condition. We use this study to identify the working frequency range of the SAW device. Due to the linear relation between the electric field and the displacement field in the piezoelectric materials, we can observe the similar distribution of the displacement field and the electric potential in the material from Figure 3.4 and 3.5. The surface wave mode of the our structure is found at 217MHz and 219MHz.

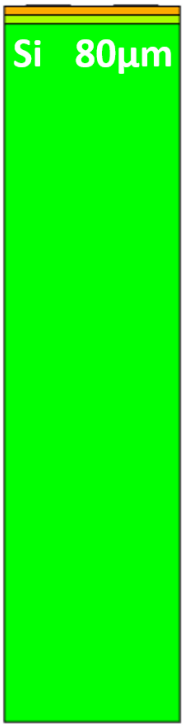

Figure 3.2: The simulated geometry of the SAW device

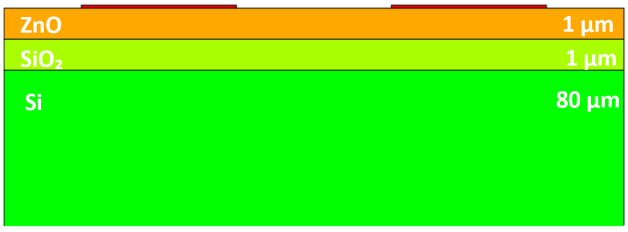

Figure 3.3: The magnified simulated geometry of the SAW device

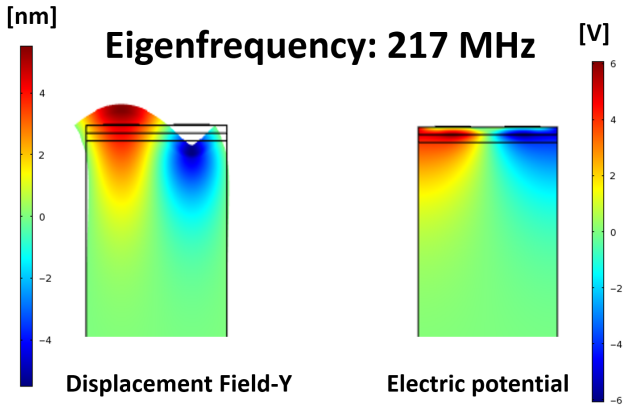

Figure 3.4: Displacement field and electric potential of eigenfrequency at 217MHz

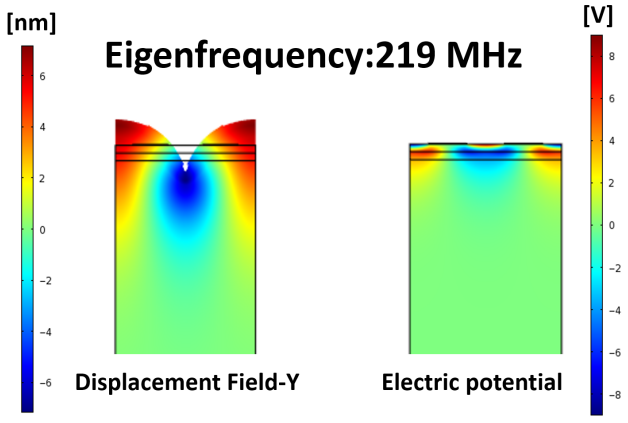

Figure 3.5: Displacement field and electric potential of eigenfrequency at 219MHz

3.3.2 Frequency Sweep Analysis

We perform the frequency sweep analysis to illustrate the acoustic wave propagation at the surface wave mode frequencies and the insertion loss of the SAW device after the eigenfrequencies of the SAW device is identified. We used SiO_2/Si as a substrate material with the same thicknesses as in the previous work. The piezoelectric material, finger width and finger space of IDTs are the same with the eigenfrequency analysis study. Delay line of the device is 65μm. Left and right sides of the devices surrounding by the virtual domains which are set as the perfectly matched layers to avoid edge reflections of the acoustic waves. Input fingers are excited with the electric potential +1V and -1V respectively, the output fingers are set as the floating potential boundary condition to receive the potential distribution under them. The geometric illustration of the device is shown in Figure 3.6. The sweep frequency range is 150-250MHz with 1MHz steps.

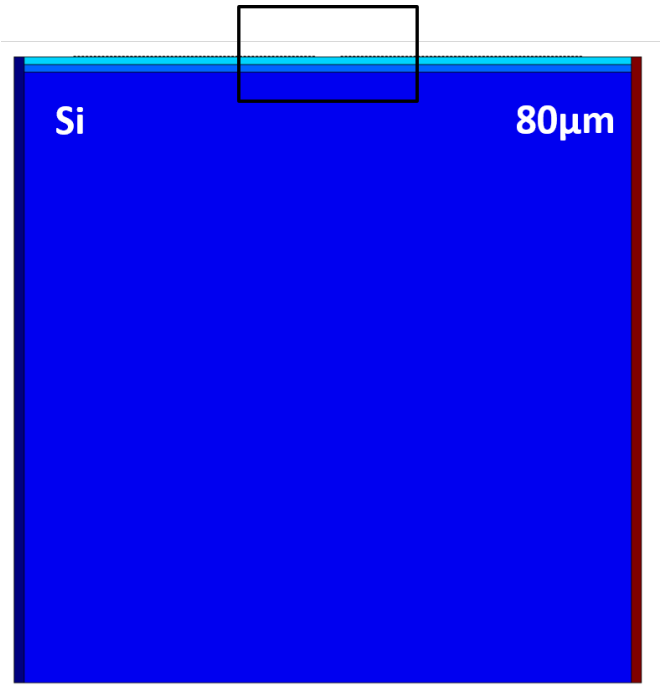

Figure 3.6: The simulated geometry of SAW device for the frequency sweep

All frequency responses were obtained, the highest potential output is generated at the frequencies near 217MHz and 219MHz. As an example of non-propagating acoustic wave Figure 3.8 is demonstrated. We can easily see the

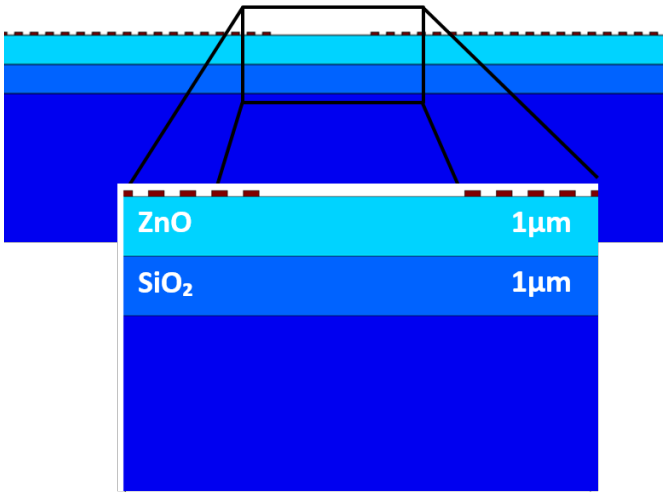

Figure 3.7: The magnified simulated geometry of SAW device for the frequency sweep

attenuation of the waves.

Figure 3.9 and 3.10 show the propagation of acoustic waves into the media. These frequencies are the surface acoustic wave interfere constructively and arrive the output fingers. After these observations we get the 1D plot of the insertion loss (explained in Section 4.1.3) which is the ratio of the output signal to the input signal. The loss is lower where the attenuation is lower. We can observe the peak around the 219MHz. Insertion loss of the devices can be seen in Figure 3.11. The insertion loss characteristics have good agreement with the simulation and the experiment results in the literature [46].

The loss around the 217MHz is nearly 40dB lower with respect to other frequencies. The acoustic wave velocity of the ZnO can be calculated using Equation 2.22 and the result is around 4340m/s. In the literature different ZnO acoustic velocities are demonstrated, it strongly depends on the film thickness and substrate material [4]. Our simulated wave velocity is very similar with the velocities of ZnO/SiO_2 structure reported in the literature (4200m/s)[4].

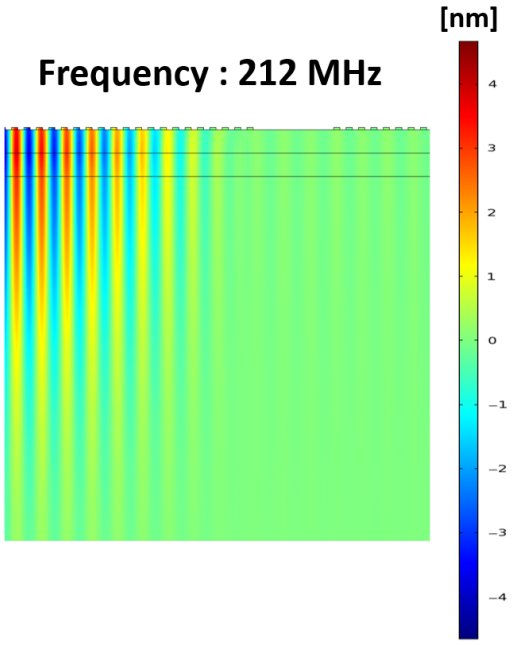

Figure 3.8: Y component of the displacement field at 212MHz

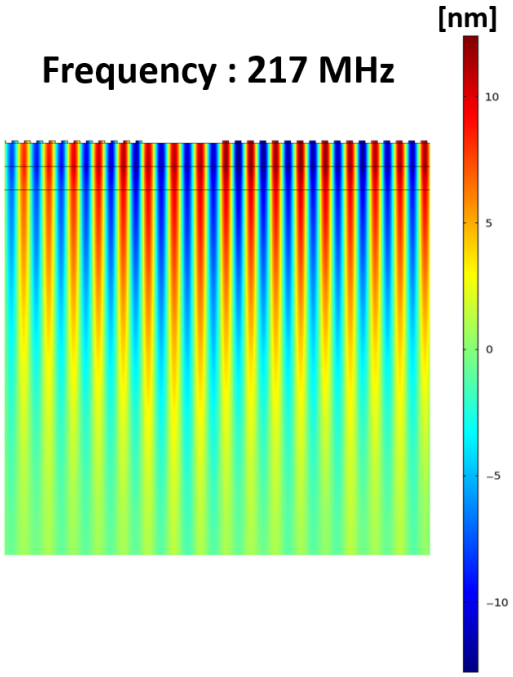

Figure 3.9: Y component of the displacement field at 217MHz

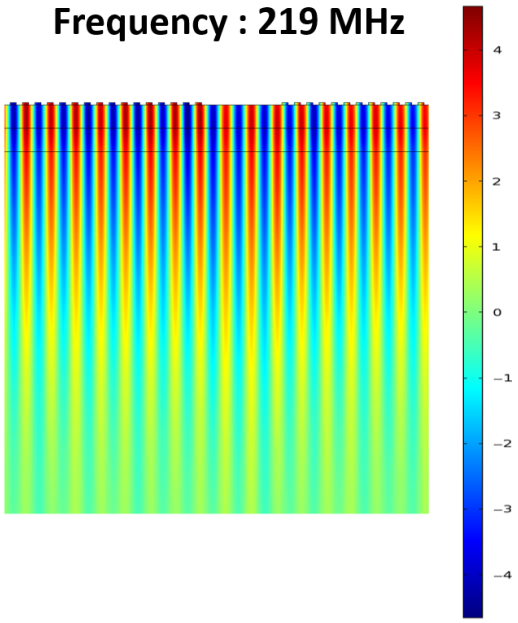

Figure 3.10: Y component of the displacement field at 219MHz

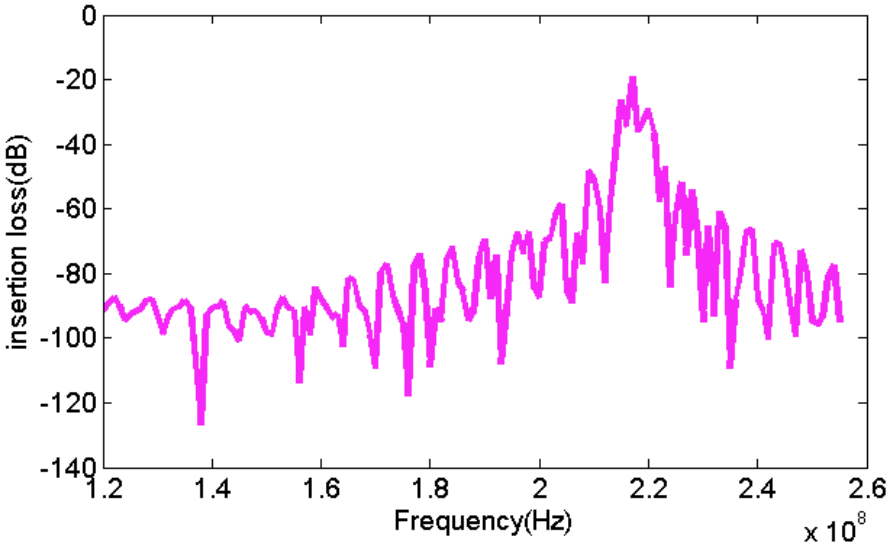

Figure 3.11: Insertion loss spectrum of the simulated device

3.3.3 Parametric Sweep Analysis

In order to analyze the effects of the design parameters parametric sweep study was made. Firstly, we studied on the film thickness sweep in the frequency sweep study and plotted the insertion loss changes with respect to film thickness. Secondly, the effect of substrate thickness is investigated. Thirdly, effect of delay line length changes is studied in the frequency sweep analysis. Finger geometry and the effect of discretization was analyzed using eigenfrequency analysis to observe a frequency shift.

3.3.3.1 Effect of ZnO Film Thickness

Thickness is one of the most important parameters that specify the acoustic wave velocity and the frequency response of the SAW device. To observe the effect of the ZnO thickness over the SAW insertion loss values we construct the parametric sweep study of the film thickness with a frequency sweep solution. Changing thickness values of the ZnO were chosen as 0.5μm, 1μm, 1.5μm and 2 μm. The results are shown in Figure 3.12.

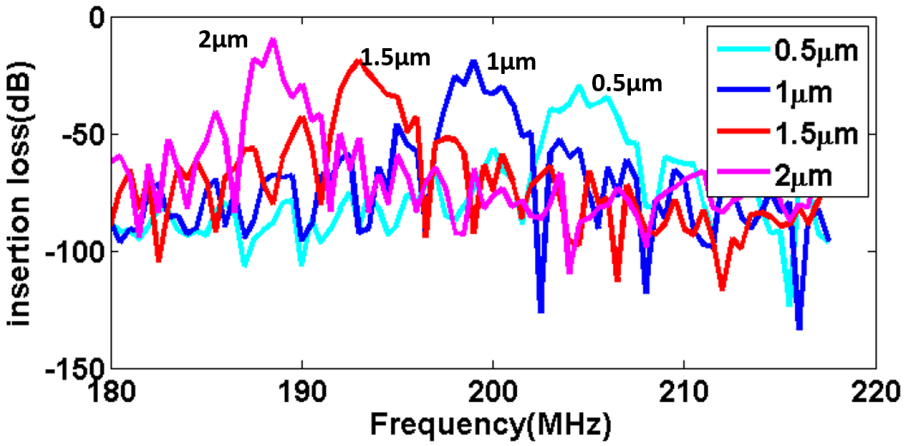

Figure 3.12: Insertion loss and resonant frequency variation with respect to different thicknesses of ZnO film

According to Figure 3.12, the resonant frequency of the SAW device decreases with increasing thickness of the ZnO film. Because the applied force or electric

field values are constant, stress values inside the film change between each film, this results in decrease in the resonance frequency. If initial stress is same for each film, resonance frequency will increase with the increasing thickness. This effect may also occur due to the acoustic velocity change with the thickness of ZnO film. The decrease in acoustic velocity of ZnO with increasing thickness is reported in literature [47]. It is stated that the acoustic velocity of Si is higher than that of ZnO and when we increase the thickness of ZnO, it is an effect on the acoustic wave increase and the overall velocity converge more to the ZnO velocity [18]. Our results are similar with the experimental results reported in the literature [18]. The decrease in the acoustic velocity results in the decrease of resonant frequency of the device.

3.3.3.2 Effect of Substrate Thickness

In our study, we choose Si substrate thickness as 80μm. Si substrates are generally 500μm in our applications. To low computational cost, Si thickness is taken as 80μm. We studied the parametric sweep of the Si substrate with the thicknesses 60μm, 70μm, 80μm, 90μm, 100μm and show that increasing Si thickness beyond 80μm does not affect the outcome.

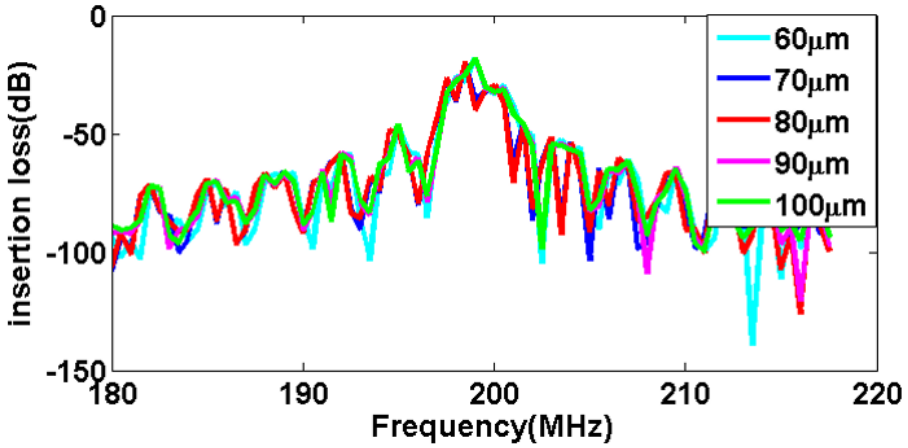

Figure 3.13: Insertion loss for different substrate thicknesses

The frequency sweep analysis is performed to observe both frequency shift and insertion loss characteristics. The insertion loss and resonant frequencies are shown in Figure3.13. Device properties are observed to be rather insensitive to substrate thickness in this range. As mentioned before in section 2.3, the penetration depth of the surface waves is nearly one wavelength.

3.3.3.3 Effect of Finger Geometry

The important parameter that defines the frequency response of the SAW device is the finger geometry. It sets the wavelength of the acoustic wave and by this way frequency response can be changed. In this study, finger widths and the finger spaces were changed. Spaces and widths are equal to each other at each study. Other parameters are kept the same with the initial structure: 80μm substrate thickness, 1μm SiO_2 thickness, 1μm ZnO thickness. Finger width and spacings are swept from 1, 3, 5, 7 to 9μms.

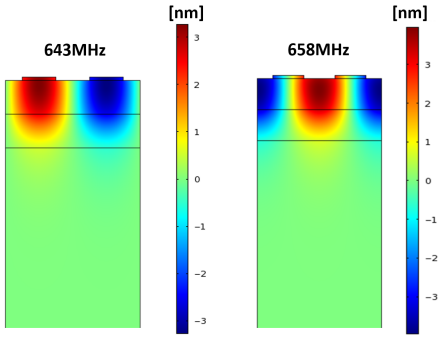

Figure 3.14: Eigenfrequencies of the device which has 1μm finger width and spacing

Figure 3.14 and 3.15 show simulated eigenfrequencies of the same modes for different thicknesses. The two fundamental eigenfrequency modes of all parameters (1, 3, 5, 7 and 9μm finger widths and spacings) exhibit resonant frequencies at 644-658MHz, 315-324MHz, 217-219MHz, 163-165MHz and 131-132MHz respectively. This decay is in well agreement with theoretical predictions and reported

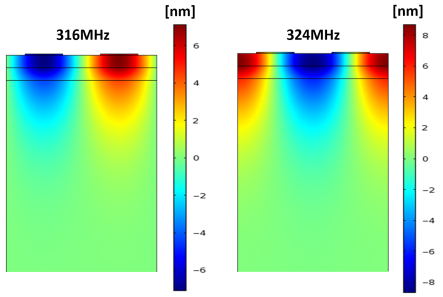

Figure 3.15: Eigenfrequencies of the device which has 3μm finger width and spacing

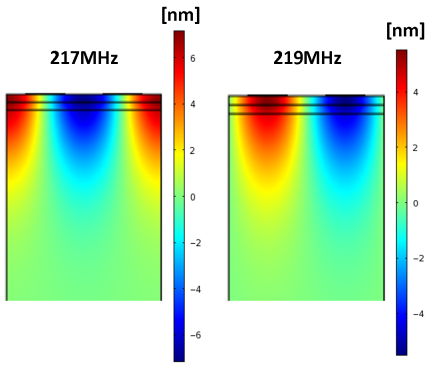

Figure 3.16: Eigenfrequencies of the device which has 5μm finger width and spacing

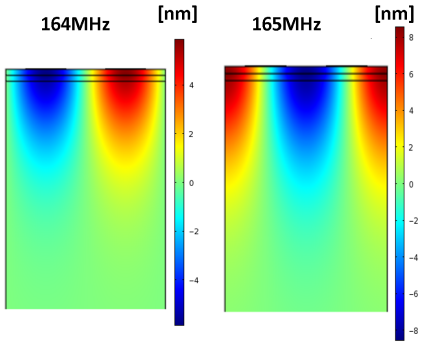

Figure 3.17: Eigenfrequencies of the device which has 7μm finger width and spacing

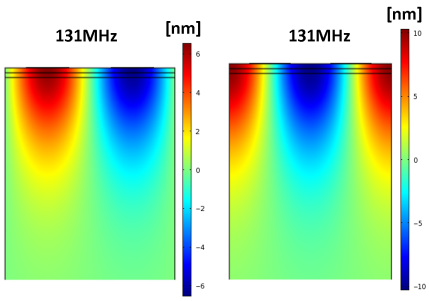

Figure 3.18: Eigenfrequencies of the device which has 9μm finger width and spacing

results in the literature [46]. The narrowing of the frequency separation as the wavelength increase is noted. This situation is reported in a similar study [46].

3.3.3.4 Effect of Discretization

Discretization divide the continuous structure to discrete elements as mentioned before in the section 3.1. Although discretization is not the parameter of the SAW devices, it is a critical parameter for the FEM simulations. Discretization determines the convergence of simulation to the reality.

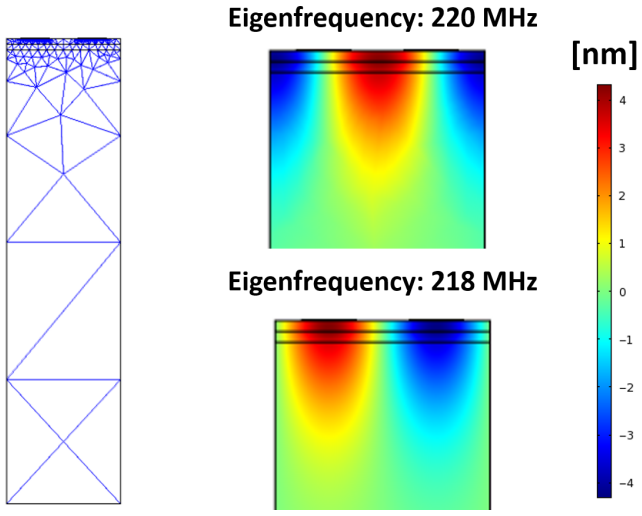

Figure 3.19: Eigenfrequency result with coarse mesh

We tested 3 types of discretization which is defined in the COMSOL as extremely coarse, normal and extremely fine. In Figure 3.19, 3.20, and 3.21, the meshed structures and the results are illustrated. We can observe how the frequency shift occurs when the number of meshing elements are increased. The increasing element number increases the computational cost of the simulations. According to the aim of the simulations meshing should be optimized.

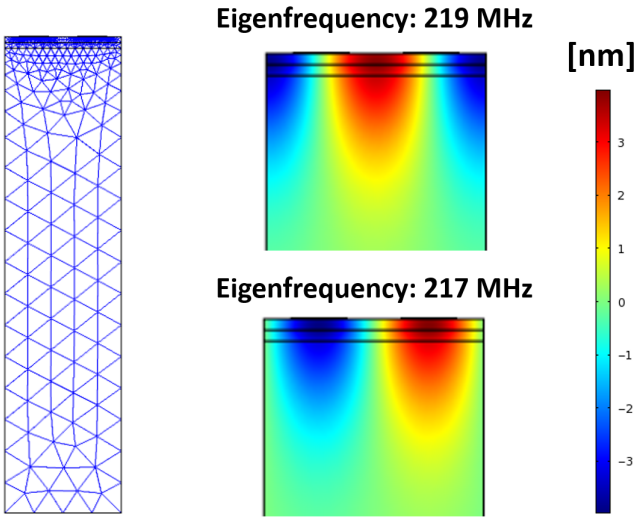

Figure 3.20: Eigenfrequency result with normal meshing

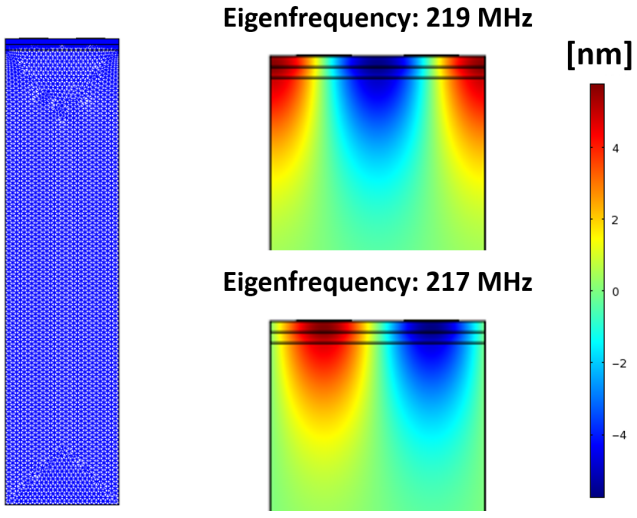

Figure 3.21: Eigenfrequency result with fine meshing

Chapter 4

Experimental Details and Results

4.1 ZnO and V-doped ZnO based SAW devices

4.1.1 Fabrication

SAW device fabrication has two steps: deposition of piezoelectric film and formation of IDT electrodes. ZnO is chosen as a piezoelectric film. ZnO is deposited on thermal oxide (SiO_2) coated Si (111) wafer by the RF magnetron sputtering method. Vaksis NanoD 4S sputtering system was used. 1μm ZnO is deposited with a deposition rate of 1.98nm/sec using a ZnO target having 99.999% purity at 150W RF power and 50sccm Ar, 10sccm O_2 gas flow under vacuum conditions. After the deposition is completed, two sets of device are prepared: post-annealed and as-deposited ZnO samples. Samples are heated to 600 °C for 30 minutes by rapid thermal annealing (RTA) system. IDT electrode metals were formed onto the annealed and as-deposited samples using lift off process. Electrode metal is gold, which is 100nm and titanium was deposited before gold as an adhesion layer with the thickness of 3nm. The IDT electrodes are formed from two sets of 30 fingers with 5μm width and 5μm finger space. Delay line of fabricated device is 65μm. Fabrication steps are illustrated in Figure 4.1 and scanning electron microscope images are shown in Figure 4.2.

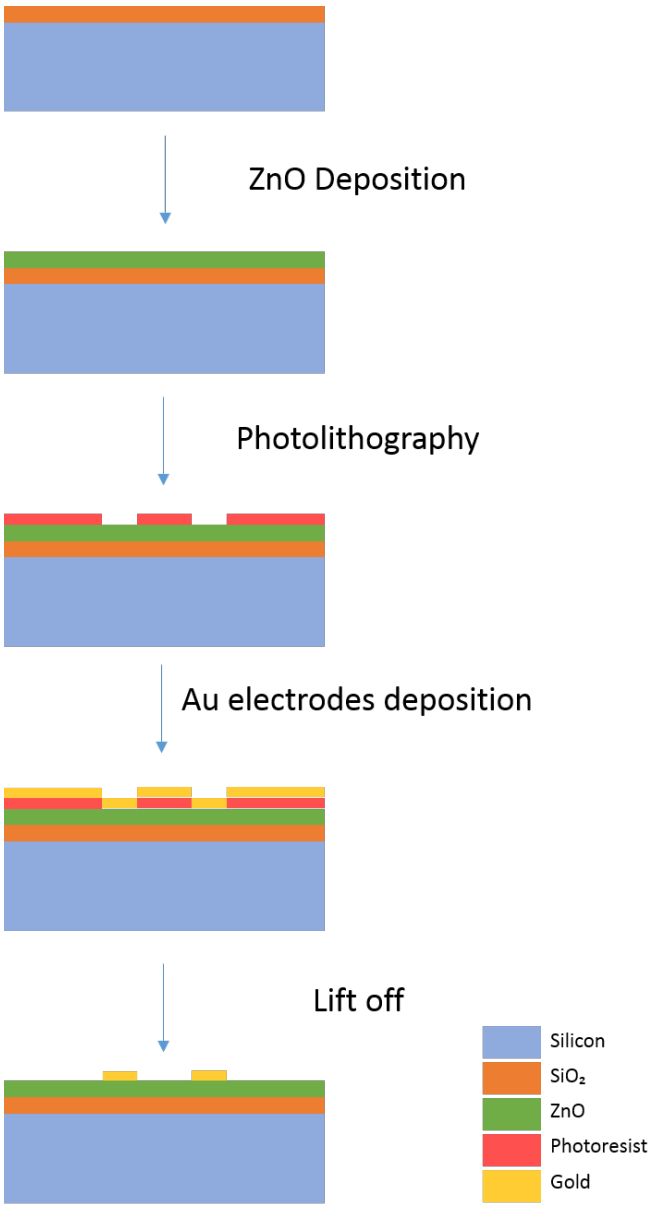

Figure 4.1: Fabrication steps of SAW device

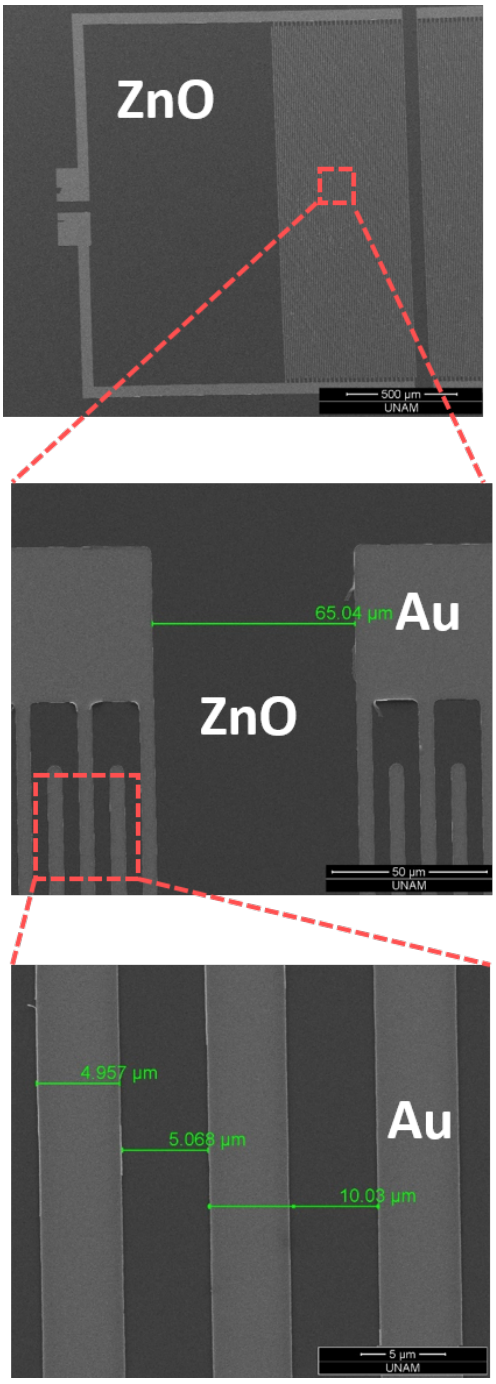

Figure 4.2: SEM images of the fabricated device

Fabrication of the device is same for the V-doped ZnO samples except the deposition step. V-doped ZnO is deposited with co-sputtering method of homogenous doping of V atoms in the ZnO crystals. ZnO and V_2O5 films are sputtered alternately. The sputtering conditions of ZnO are the same with the other samples. V_2O_5 is sputtered by DC reactive magnetron sputtering with 150W DC power, 40sscm Ar gas flow, 10mTorr base pressure under vacuum conditions. The V_2O_5 film deposition rate is 2nm/sec. V-doped ZnO samples were annealed at 350 °C (since melting point of V_2O_5 is 690 °C).

4.1.2 Material Characterization Results of Sputtered ZnO and V-doped ZnO thin films

Material characterization of the four types of samples is performed with X-ray diffraction spectroscopy (XRD) for crystallinity analysis and X-ray photoelectron spectroscopy (XPS) for the elemental analysis.

4.1.2.1 XRD Results

In this work, we analyze the effect of V-doping and annealing on the sputtered ZnO. The X-ray diffraction peaks are identified using a Pananalytical (Xpert Pro MPD) XRD instrument. In literature, it is reported that annealing of ZnO increase the wurtzite peaks of the films (00l) [48].

In Figure 4.3 XRD patterns of annealed ZnO, as deposited ZnO, as deposited V-doped ZnO and annealed V-doped ZnO are shown. XRD profile of annealed and as-deposited V-doped ZnO is similar but we observe the V_2O_5 600 peaks in addition to ZnO 00l peaks. 002 peaks of V-doped samples are higher than ZnO samples. As a result of XRD analysis, we conclude that a multilayer structured thin film ZnO/V_2O_5 is obtained instead of V-doped ZnO and V_2O_5 layer increased the 002 orientation of ZnO films.

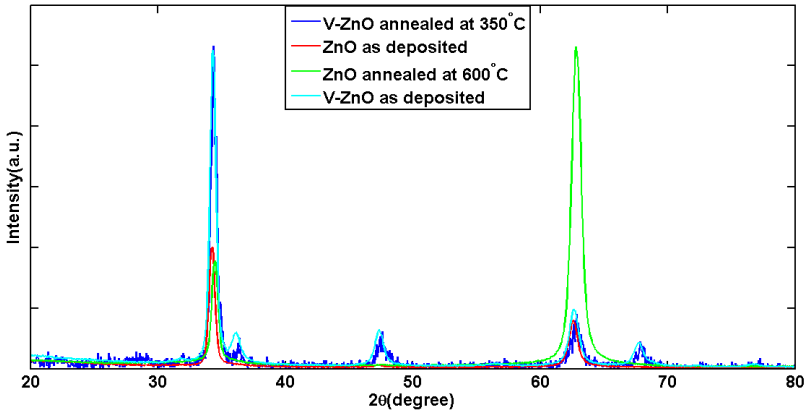

Figure 4.3: XRD result of different samples

4.1.2.2 XPS Results

The chemical composition and bonding states of the V-ZnO films are analyzed via XPS, using a Thermo Scientific K-Alpha device with a monochromatized Al K X-ray source.

The atomic percentage ratios of the scanned survey are shown in Table 4.1.

Table 4.1: The atomic percentage ratios of the scanned survey

	Zn	O	V	C
Atomic Percentage	23.19	56.08	9.29	11.47

Table 4.2: V_xO_y and ZnO bonding states for O1s and V2p3/2 bonding states

	Peak BE(eV)	FHWM	Area
O1s(V_2O_5)	530	1.92	59404.20
V2$p_{1/2}$(V_2O_5)	1.17	1.92	21007.89
V2$p_{1/2}$(V_2O_3)	0.66	1.92	1832.14
O1s(ZnO)	532.6	0.85	2039.32
V2$p_{1/2}$(V_2O_3)	515.2	0.71	1134.84

Depth profile analysis of the films are performed via in-situ etching with constant time intervals (120s) with a beam of Ar ions in ultra-high vacuum condition. Figure 4.4 shows the atomic percentage of the V-ZnO films with respect to the etch time. As shown in the figure the atomic percentage of the V is around 1%

inside ZnO film. At around 2000s corresponding to the etch level of 17, the V concentration is again around 9%.

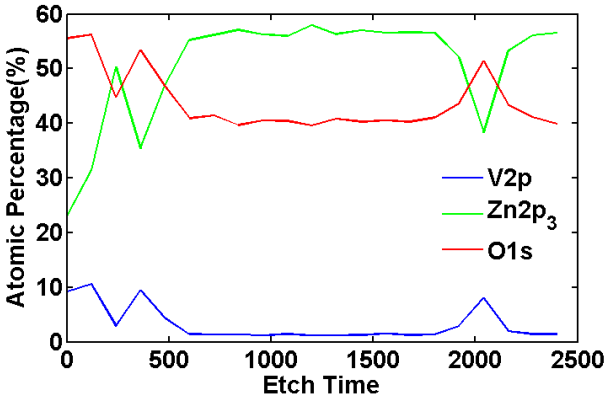

Figure 4.4: Atomic percentage profile with respect to the etch time.

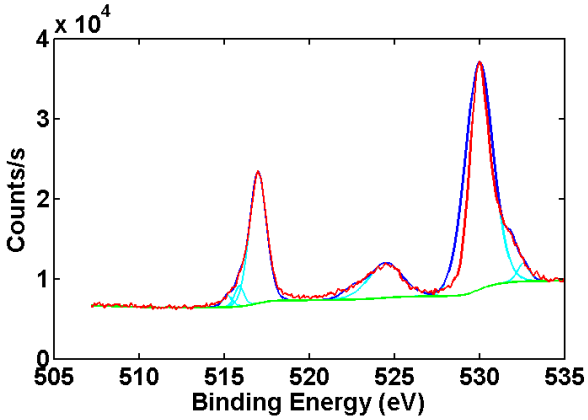

Figure 4.5: Vanadium fitting

The binding energy of the V2p core level depends on the oxidation state of the V ions. In the literature, most of the authors analyzed the bonding states of vanadium ions by taking into account only V2p3/2 signals. Figure 4.5 shows the curve fitting of VO_x with including O1s signal to analyze the Shirley background. Our fitting curves match with the reported VO_x and ZnO bonding states for O1s and V2p3/2 bonding states shown in the Table 4.2. Our film includes both V_2O_3 and V_2O_5 states.

4.1.3 Measurement Setup

Fabricated device frequency response characterization was conducted with vector network analyzer (VNA) (Agilent E8361A PNA) and Cascade Microtech ACP40-A (GSG, 150 um pitch) probes. Network analyzer involves signal generator, test set and receiver parts. Signal generator provides a test signal, test set takes this signal and applies it to the device, then it sends measured signal to the receiver which calculates the amplitude and phase of signals. Our devices have two ports and we performed the scattering parameter (S-Parameter) measurement. There are four S-parameters: $S_{11}, S_{12}, S_{21}, S_{22}$.

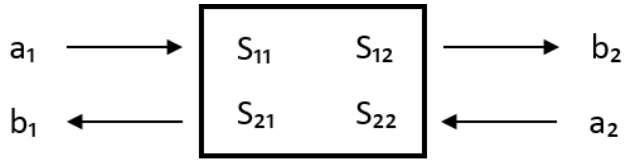

Figure 4.6: S-parameters

S_{11} : the measure of reflected signal from input port.

S_{22} : the measure of reflected signal from output port.

S_{12} : the ratio of input signal from port 1 to the transmitted signal to port 2.

S_{21}: the ratio of the received signal from port 2 to input signal from port 1.

$$\begin{pmatrix} b_1 \\ b_2 \end{pmatrix} = \begin{pmatrix} S_{11} & S_{12} \\ S_{21} & S_{22} \end{pmatrix} \begin{pmatrix} a_1 \\ a_2 \end{pmatrix} \tag{4.1}$$

The relation between S-parameters are given in Equation 4.1. a_1, a_2 denotes the incident waves at port 1 and port 2 respectively, and b_1, b_2 denotes the reflected waves from port 1 and port 2 respectively.

Insertion loss (IL) of the device can be calculated from S_{21} parameter by Equation 4.2 in the log scale.

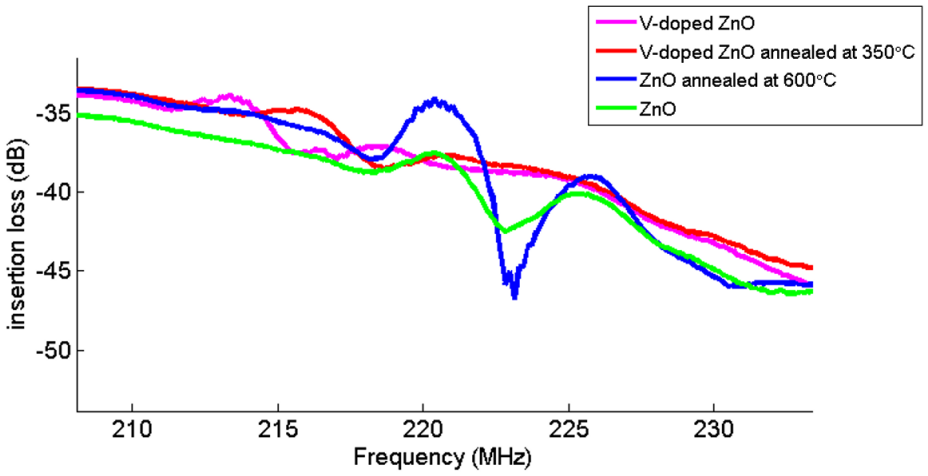

Figure 4.7: Insertion loss of fabricated devices

$$IL = 20log_{10}|S_{21}| \tag{4.2}$$

If there is no amplification, the S parameters can be between 0 and 1 value in decimal scale, due to the two boundaries, either full reflection or full transmission. In the logarithmic scale, if there is a full reflection, IL become equals to $-\infty$, and if there is a full transmission it equals to 0. From this point of view, our devices IL and their characteristics will be discussed in the next section.

4.2 Results and Discussion

We fabricated identical devices on different piezoelectric substrates. IDT finger widths and spacings are 5μm ($\lambda = 20\mu$m). The propagation length is 10μm. Number of finger pairs are 30. In this study IDT design is not variable. The influence of different substrates and annealing is presented. Our substrates are ZnO, annealed ZnO, V-doped ZnO, annealed V-doped ZnO. Annealing temperature of ZnO and V-doped ZnO is 600°C and 350°C respectively. S_{21} measurements of four different devices were performed. Results are shown in Figure 4.7.

These results reveal that annealed ZnO has the best performance with -34.05dB insertion loss at its resonant frequency 219MHz. Insertion loss of as deposited ZnO is -37.61dB, lower than the insertion loss of annealed ZnO. Their resonant frequencies are the same. This difference may be the result of an increase in the piezoelectric response of ZnO with annealing.

The insertion losses of V-doped ZnO and annealed V-doped ZnO are -33.85dB and -34.79dB with the resonant frequencies 213MHz and 215MHz respectively. Their performance is better than the as deposited ZnO. Annealing did not make a remarkable change in the insertion loss levels of the V-doped ZnOs. Their frequencies are shifted after annealing, it may not be the effect of annealing because their XPS and XRD results are very similar, it may be due to non uniformity of sputtered films since the resonant frequencies can be shifted by thickness.

The insertion loss levels of annealed ZnO and V-doped ZnOs are close to that of as deposited ZnO. It can be deduced that piezoelectric responses of these films are similar.

The resonant frequencies of the ZnO and annealed ZnO are consistent with the simulation results, although the amplitudes of experimental ones are lower due to the polycrystalline structure of the deposited films whereas a single crystal structure is assumed for the simulations.

Chapter 5

Conclusions and Future Directions

Piezoelectric materials are used in electrical and mechanical energy conversion based devices such as microphones, accelerometers, speakers, hydrophones, pressure sensors etc. Thin film piezoelectric materials are promising due to their MEMS and CMOS compatibility. Among thin films, ZnO is attractive material due to giant piezoelectricity when it is doped with vanadium.

SAW devices are one of the piezoelectric thin film applications. SAW devices are formed by a pair of interdigitated transducers (IDTs) and input and output IDTs. IDTs are fabricated onto the piezoelectric thin film. Applied oscillating electric field from input IDT creates surface acoustic waves in the piezoelectric thin film and these acoustic waves are converted back into an electrical signal at the output IDT.

This thesis presents the 2D COMSOL simulations of ZnO based SAW devices. We invesitage the parameters that affect the SAW device performances by simulations. These parameters are finger geometry, film thickness, substrate thickness and discretization.

V doping of ZnO is realized with sequential deposition of V_2O_5 and ZnO films.

XRD and XPS results verified precense of vanadium. Our films have structures similar to V_2O_5. SAW devices were fabricated onto these films. The measurement results show the insertion loss levels of V-doped ZnO films and annealed ZnO films are similar although the frequencies are shifted.

The resonant frequencies of the fabricated devices are consistent with the simulated ones, although the insertion losses of fabricated devices are much smaller due to the material properties of simulated ZnO.

For the future application, the design and fabrication of SAW devices will be optimized. V doping of ZnO will be realized with co-sputtering method. V_2O_5 can be used as interlayer between the substrate and ZnO to improve the crystal quality of ZnO. In simulations, the effect of different material properties may be analyzed. SAW filters or gas sensing devices may be produced with proper design and fabrication.

Bibliography

[1] C. Ahn, K. Rabe, and J.-M. Triscone, "Ferroelectricity at the nanoscale: local polarization in oxide thin films and heterostructures," *Science*, vol. 303, no. 5657, pp. 488–491, 2004.

[2] E. F. Morgan and M. L. Bouxsein, "Use of finite element analysis to assess bone strength," *BoneKEy-Osteovision*, vol. 2, no. 12, pp. 8–19, 2005.

[3] M. Fraga, H. Furlan, R. Pessoa, and M. Massi, "Wide bandgap semiconductor thin films for piezoelectric and piezoresistive mems sensors applied at high temperatures: an overview," *Microsystem Technologies*, vol. 20, no. 1, pp. 9–21, 2014.

[4] V. Mortet, O. Williams, and K. Haenen, "Diamond: a material for acoustic devices," *physica status solidi (a)*, vol. 205, no. 5, pp. 1009–1020, 2008.

[5] A. Manbachi and R. S. Cobbold, "Development and application of piezoelectric materials for ultrasound generation and detection," *Ultrasound*, vol. 19, no. 4, pp. 187–196, 2011.

[6] G. Lippmann, "Principe de la conservation de l'électricité, ou second principe de la théorie des phénomènes électriques," *J. Phys. Theor. Appl.*, vol. 10, no. 1, pp. 381–394, 1881.

[7] S. Katzir, "Who knew piezoelectricity? rutherford and langevin on submarine detection and the invention of sonar," *Notes and Records of the Royal Society*, p. rsnr20110049, 2012.

[8] P. Dineva, D. Gross, R. Müller, and T. Rangelov, "Dynamic fracture of piezoelectric materials," *AMC*, vol. 10, p. 12, 2014.

[9] Y. Zhang, Y. Liu, and Z. L. Wang, "Fundamental theory of piezotronics," *Advanced Materials*, vol. 23, no. 27, pp. 3004–3013, 2011.

[10] P. Muralt, "Ferroelectric thin films for micro-sensors and actuators: a review," *Journal of Micromechanics and Microengineering*, vol. 10, no. 2, p. 136, 2000.

[11] A. Kholkin, N. Pertsev, and A. Goltsev, "Piezoelectricity and crystal symmetry," in *Piezoelectric and Acoustic Materials for Transducer Applications*, pp. 17–38, Springer, 2008.

[12] Y. Fu, J. Luo, X. Du, A. Flewitt, Y. Li, G. Markx, A. Walton, and W. Milne, "Recent developments on zno films for acoustic wave based bio-sensing and microfluidic applications: a review," *Sensors and Actuators B: Chemical*, vol. 143, no. 2, pp. 606–619, 2010.

[13] O. Kluth, G. Schöpe, J. Hüpkes, C. Agashe, J. Müller, and B. Rech, "Modified thornton model for magnetron sputtered zinc oxide: film structure and etching behaviour," *Thin solid films*, vol. 442, no. 1, pp. 80–85, 2003.

[14] M. Koch, A. Hartmann, R. Lamb, M. Neuber, and M. Grunze, "Self-texture in the initial stages of zno film growth," *The Journal of Physical Chemistry B*, vol. 101, no. 41, pp. 8231–8236, 1997.

[15] Y. E. Lee, Y. J. Kim, and H. J. Kim, "Thickness dependence of microstructural evolution of zno films deposited by rf magnetron sputtering," *Journal of materials research*, vol. 13, no. 05, pp. 1260–1265, 1998.

[16] W. T. Lim, B. K. Son, D. H. Kang, and C. H. Lee, "Structural properties of aln films grown on si, ru/si and zno/si substrates," *Thin Solid Films*, vol. 382, no. 1, pp. 56–60, 2001.

[17] T. Lamara, M. Belmahi, O. Elmazria, L. Le Brizoual, J. Bougdira, M. Remy, and P. Alnot, "Freestanding cvd diamond elaborated by pulsed-microwave-plasma for zno/diamond saw devices," *Diamond and related materials*, vol. 13, no. 4, pp. 581–584, 2004.

[18] X. Du, Y. Fu, S. Tan, J. Luo, A. Flewitt, W. Milne, D. Lee, N. Park, J. Park, Y. Choi, *et al.*, "Zno film thickness effect on surface acoustic wave modes and acoustic streaming," *Applied Physics Letters*, vol. 93, no. 9, p. 094105, 2008.

[19] F. Pan, C. Song, X. Liu, Y. Yang, and F. Zeng, "Ferromagnetism and possible application in spintronics of transition-metal-doped zno films," *Materials Science and Engineering: R: Reports*, vol. 62, no. 1, pp. 1–35, 2008.

[20] S. Wolf, D. Awschalom, R. Buhrman, J. Daughton, S. Von Molnar, M. Roukes, A. Y. Chtchelkanova, and D. Treger, "Spintronics: a spin-based electronics vision for the future," *Science*, vol. 294, no. 5546, pp. 1488–1495, 2001.

[21] J. Coey, M. Venkatesan, and C. Fitzgerald, "Donor impurity band exchange in dilute ferromagnetic oxides," *Nature materials*, vol. 4, no. 2, pp. 173–179, 2005.

[22] T. Dietl, H. Ohno, F. Matsukura, J. Cibert, and D. Ferrand, "Zener model description of ferromagnetism in zinc-blende magnetic semiconductors," *Science*, vol. 287, no. 5455, pp. 1019–1022, 2000.

[23] Y. Yang, C. Song, X. Wang, F. Zeng, and F. Pan, "Cr-substitution-induced ferroelectric and improved piezoelectric properties of zn1- xcrxo films," *Journal of Applied Physics*, vol. 103, no. 7, p. 074107, 2008.

[24] Y. Yang, C. Song, X. Wang, F. Zeng, and F. Pan, "Giant piezoelectric d 33 coefficient in ferroelectric vanadium doped zno films," *Applied Physics Letters*, vol. 92, no. 1, pp. 012907–012907, 2008.

[25] D. Ballantine Jr, R. M. White, S. J. Martin, A. J. Ricco, E. Zellers, G. Frye, and H. Wohltjen, *Acoustic Wave Sensors: Theory, Design, & Physico-Chemical Applications*. Academic press, 1996.

[26] D. V. Hutton, *Fundamentals of finite element analysis*. McGraw-Hill Science/Engineering/Math, 2003.

[27] R. W. Clough, "The finite element method in plane stress analysis," 1960.

[28] P. E. Grafton and D. Stome, "Analysis of axisymmetrical shells by the direct stiffness method," *AIAA journal*, vol. 1, no. 10, pp. 2342–2347, 1963.

[29] E. L. Wilson, "Structural analysis of axisymmetric solids.," *AIAA Journal*, vol. 3, no. 12, pp. 2269–2274, 1965.

[30] H. C. Martin, "Finite element analysis of fluid flows," tech. rep., DTIC Document, 1968.

[31] E. L. Wilson and R. E. Nickell, "Application of the finite element method to heat conduction analysis," *Nuclear Engineering and Design*, vol. 4, no. 3, pp. 276–286, 1966.

[32] R. H. MacNeal, *The NASTRAN theoretical manual*, vol. 1. Scientific and Technical Information Office, National Aeronautics and Space Administration, 1972.

[33] S. Moaveni, *Finite element analysis: theory and application with ANSYS*. Pearson Education India, 2003.

[34] A. I. Manuals, "Algor finite element analysis system," 2000.

[35] M. Lashkari, "Cosmos/m user guide," *Volume II. release*, vol. 1, no. 6, 1992.

[36] C. Multiphysics, "3.4, comsol inc," *Burlington, MA*, 2005.

[37] G. Endoh, K.-y. Hashimoto, and M. Yamaguchi, "Surface acoustic wave propagation characterisation by finite-element method and spectral domain analysis," *Japanese journal of applied physics*, vol. 34, no. 5S, p. 2638, 1995.

[38] N. Rama Krishnan, H. B. Nemade, and R. Paily, "Simulation of one-port saw resonator using comsol multiphysics,"

[39] L. Le Brizoual, F. Sarry, F. Moreira, and O. Elmazria, "Fem modelling of surface acoustic wave in diamond layered structure," *physica status solidi (a)*, vol. 203, no. 12, pp. 3179–3184, 2006.

[40] N. R. Krishnan, H. B. Nemade, and R. Paily, "Simplified finite element simulation of a saw hydrogen sensor using comsol multiphysics," *Excerpt Proc. COMSOL*, 2008.

[41] L. Le Brizoual, F. Sarry, O. Elrnazria, P. Alnot, S. Ballandras, and T. Pastureaud, "Ghz frequency zno/si saw device," *Ultrasonics, Ferroelectrics and Frequency Control, IEEE Transactions on*, vol. 55, no. 2, pp. 442–450, 2008.

[42] Y. Rao and G. Zhang, "3d modeling of a surface-acoustic-wave based sensor," in *COMSOL Conference*, 2007.

[43] G. Zhang, "Nanostructure-enhanced surface acoustic waves biosensor and its computational modeling," *Journal of Sensors*, vol. 2009, 2009.

[44] G.-S. Chung and D.-T. Phan, "Finite element modeling of surface acoustic waves in piezoelectric thin films," 2010.

[45] S. Büyükköse, B. Vratzov, D. Ataç, J. van der Veen, P. Santos, and W. van der Wiel, "Ultrahigh-frequency surface acoustic wave transducers on zno/sio2/si using nanoimprint lithography," *Nanotechnology*, vol. 23, no. 31, p. 315303, 2012.

[46] H. Jin, J. Zhou, X. He, W. Wang, H. Guo, S. Dong, D. Wang, Y. Xu, J. Geng, J. Luo, *et al.*, "Flexible surface acoustic wave resonators built on disposable plastic film for electronics and lab-on-a-chip applications," *Scientific reports*, vol. 3, 2013.

[47] X. Du, Y. Fu, S. Tan, J. Luo, A. Flewitt, S. Maeng, S. Kim, Y. Choi, D. Lee, N. Park, *et al.*, "Zno film for application in surface acoustic wave device," in *Journal of Physics: Conference Series*, vol. 76, p. 012035, IOP Publishing, 2007.

[48] V. Gupta and A. Mansingh, "Influence of postdeposition annealing on the structural and optical properties of sputtered zinc oxide film," *Journal of Applied Physics*, vol. 80, no. 2, pp. 1063–1073, 1996.